Crack Path Bifurcation at a Tear Strap in a Pressurized Stiffened Cylindrical Shell

Amy L. Cowan

Thesis submitted to the Faculty of the
Virginia Polytechnic Institute and State University
in partial fulfillment of the requirements for the degree of

Masters of Science
in
Aerospace Engineering

Eric R. Johnson, Chair
Rakesh Kapania
Alfred C. Loos

August 24, 1999
Blacksburg, Virginia

Keywords: crack bifurcation, tear straps, pressurized shells

Crack Path Bifurcation at a Tear Strap in a Pressurized Stiffened Cylindrical Shell

Amy L. Cowan

(ABSTRACT)

A finite element model of a fracture test specimen is developed using the STAGS computer code (STructural Analysis of General Shells). The test specimen was an internally pressurized, aluminum cylindrical shell reinforced with two externally bonded aluminum tear straps around its circumference. The shell contained an initial, axial through-crack centered between the straps. The crack propagated slowly in the axial direction as the pressure increased above a certain value until a maximum pressure was attained, and then the crack propagated dynamically. The tear straps sufficiently toughened the shell such that the dynamic crack path bifurcated near the edges of the straps. The bifurcated crack branches ran circumferentially, parallel to the straps causing the shell wall to flap open.

The STAGS analysis for the static equilibrium configurations of the fractured shell include geometric nonlinearity and elastic-plastic material behavior. The crack tip opening angle (CTOA) is used in the criterion for ductile crack growth, and the critical value of the CTOA is determined by correlating the STAGS predictions of the stable portion of the crack growth curve (internal pressure versus half crack length) to the test. With the employment of a new STAGS algorithm, the complete axial crack growth curve, including both the stable and unstable portions, through the tear strap is obtained. The complete axial crack growth curve indicates that crack growth through the strap is unlikely. STAGS models with long cracks which bifurcate at various half crack lengths are developed to assess the location of crack bifurcation. Three different stress based crack turning criteria are investigated from the axial crack growth results as a second method for assessing a location of bifurcation. The bifurcation analyses and stress based turning criteria corroborate the experimentally measured bifurcation point. A parametric study is then conducted to determine the influence of tear strap thickness and width on the location of crack bifurcation.

Acknowledgements

This work was sponsored by NASA Grant NAG-1-2035.

I wish to thank Dr. James Starnes of the NASA Langley Research Center (LaRC), the technical monitor, for his assistance and allowing me to work at LaRC for extended periods of time throughout my graduate study, Dr. Carlos Dávila for hours of discussion and playing an instrumental role in guiding this work, Dr. Rick Young for assistance with the STAGS code, and Mr. Allen Waters for performing and discussing details of the fracture test. Mr. Wayne Huling of Computer Sciences Corporation was very helpful with system administration.

I would also like to extend many thanks to my advisor, Dr. Eric Johnson for making this work possible. I am very grateful for all of his advice concerning this thesis and guidance regarding all other aspects of graduate study. The Department of Aerospace and Ocean Engineering is thanked for the fellowship money I received during my two years at Virginia Tech. Dr. Rakesh Kapania and Dr. Alfred Loos are also thanked for agreeing to serve on my committee.

Finally, I would like to thank my friends and family for all their love and support while I have been pursuing this degree.

Table of Contents

List of Figures

List of Tables

CHAPTER 1

Introduction – Fracture of Pressurized Fuselage Structure

1.1 Fatal Pressure Cabin Factures

Fatigue cracking of metallic fuselage structure is an important issue in the airworthiness considerations of all transport aircraft. The destruction of aircraft caused by fatigue cracking in the fuselage has claimed many lives. Only after aircraft designs began to incorporate a pressurized cabin did the importance of this problem come into focus. Unfortunately, the combination of fatigue cracking and a pressurized fuselage has been the cause of two of the most highly publicized accidents in aviation history.

The first major aircraft accident due to fatigue cracking in a pressurized fuselage occurred in the early months of 1954. In separate accidents, two Comet I passenger jets broke apart at altitudes 30,000 feet or greater and crashed into the Mediterranean Sea. As a result of these crashes, an intensive investigation was launched. It was determined that the cause of these accidents was a result of cracks initiating at the corners of the square windows in the fuselage due to low cycle fatigue.[1,2] The window corner is a stress raiser, and under repeated tension loading of the fuselage skin due to cabin pressurization cycles, the very small cracks near the corners of the windows coalesced to form a large crack, which after reaching a critical length, propagated in an unstable manner to destroy the structural integrity of the aircraft.

More recently, another well known aircraft accident due to fatigue cracking in a pressurized fuselage occurred in 1988 during a flight of an Aloha Airline Boeing 737.[3,4,5] An investigation into this accident determined its cause originated from the large stress concentrations in the countersunk rivet holes which lead to multi-site damage, abbreviated MSD, in the aircraft skin. Eventually these MSD cracks coalesced, forming a large crack which propagated rapidly and resulted in an 18-foot section of the fuselage to be ripped away.

1.2 Mechanics of Crack Propagation in a Fuselage

While the formation of the large cracks in the previously mentioned accidents were different, the mechanics behind the crack propagation is the same. The loading condition which most influenced the crack growth is the cabin pressure. The effect of pressure on crack growth is evinced by comparing three accidents involving two DC-6 aircraft and a DC-7 aircraft which occurred near the same time as the Comet I crashes.[2] In these incidents engine problems resulted in thrown propeller blades penetrating through the fuselage. The first of these accidents occurred during a flight while the fuselage differential pressure was 4.16 psi and, in the second accident, while the fuselage differential pressure was 5.1 psi. In both accidents the fuselage differential pressure was less than 8.25 psi, the nominal fuselage operating pressure of the Comet I. The third accident occurred on the ground with the fuselage unpressurized. The damage to the fuselage that was not pressurized was only a thin slot while the two pressurized aircraft suffered 250 ft^2 and 80 ft^2 openings, respectively. This comparison further points out that the tension loading of the fuselage skin due to cabin pressurization is the critical load condition.

A pressurized, cylindrical fuselage shell containing a through crack behaves differently than a flat plate containing a through crack subjected to pressure, because of the curvature of the former with respect to the latter. With the crack oriented in the axial direction, the cylindrical fuselage shell responds by bulging. Bulging, shown in Fig. 1.1, is a deformation pattern involving both in plane displacements and large out of plane displacements in the vicinity of the crack.[2,6] These large out of plane displacements are caused by the loss of the hoop stress component along the free edge of the crack face. To

resist the pressure in the presence of the axial crack, the bulging causes panel curvature in the axial direction, which in turn permits a significant axial stress, or bulge stress as it is sometimes called, to develop in the skin in order to maintain equilibrium. The bulge stress acts parallel to the crack face.

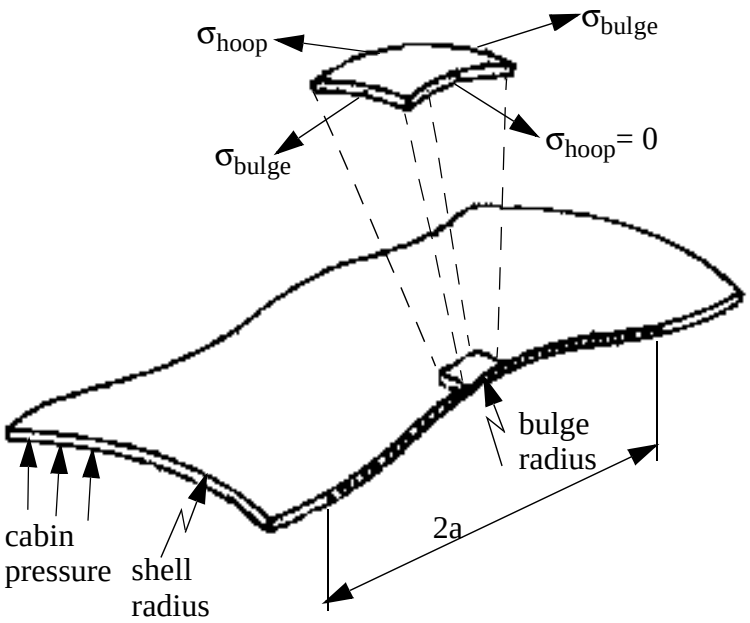

Fig. 1.1 Bulging due to an axial crack.[2]

A second phenomenon that occurs due to curvature in thin cylindrical shells containing a longitudinal crack is known as flapping. As fast crack growth propagates longitudinally at the critical internal pressure, the bulge stress increases while the hoop stress remains constant[2]. When the bulge stress became greater than the hoop stress, the crack turns in the circumferential direction, and this turning of the crack results in a portion of the shell wall to flap open. The opening of the shell wall due to the crack turning is called flapping. See Fig. 1.2. In an unstiffened pressurized cylindrical shell, flapping has been observed when the longitudinal crack becomes very long.[2] The advantage of flapping is the nonexplosive decompression of the fuselage. A slower rate of decompression would

remove the crack driving force, hopefully leading to crack arrest, while leaving the structure with some of its structural integrity intact.

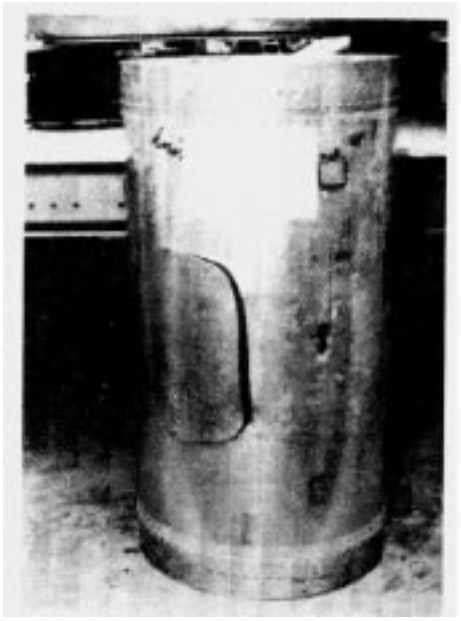

Fig. 1.2 Flapping due to crack turning.[2]

1.3 The Tear Strap

As a result of the investigations into the accidents in the 1950's, aircraft manufacturers began to incorporate into their fuselage designs features which would increase the ability of the aircraft to sustain damage caused by fatigue cracking; i.e., a damage tolerant design philosophy. A reinforced doubler on the inside of the fuselage skin, termed tear strap, crack stopper strap, or fail-safe strap, is commonly employed. Tear straps are simply strips of material attached circumferentially to the skin of the fuselage which capitalize on the advantage of flapping. A tear strap locally reduces the hoop stress thus causing the bulge stress to become greater than the hoop stress for an axial crack length that is less than the axial crack length for flapping the unstiffened cylinder. Properly designed tear straps are able to induce flapping and contain the damage between two tear straps.

These tear straps are fabricated from aluminum or titanium and are placed either between the frames as shown in Fig. 1.3a, or at the frames as shown in Fig. 1.3b.[7] It appears that the dimensions of the tear straps were, and even are to this day, determined

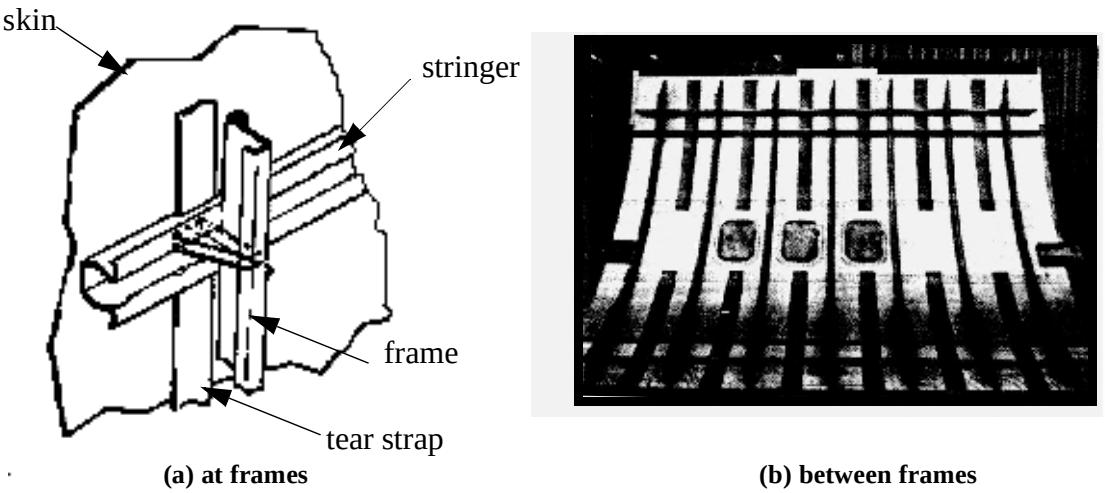

Fig. 1.3 Tear strap configurations.[7]

largely by experiment. An example of the development of fail safe features is discussed for the DC-10 by T. Swift.[8] Due to the high cost of full-scale testing, curved panels or laboratory scaled cylinders are studied to first gain an understanding basic mechanics of the problem.

1.4 Previous Fractured Cylindrical Shell Studies

The problem of an axially propagating crack in an aircraft fuselage, idealized as a perfect, circular cylindrical shell, has been the focus of numerous studies. Literature on this topic appeared after the Comet I crashes. It was in this period that Folias[9] derived the classical solutions for fractured, unstiffened, pressurized cylindrical shells. These exact solutions calculated the stress field surrounding the crack tip. Duncan and Sanders[10] performed a theoretical study of a pressurized cylindrical shell with an axial crack and a circumferential stiffener. Their study showed a circumferential stiffener affected the stresses near the crack tips only when the tip was near the stiffener.

During the 70's and 80's much work had been done in the area of pressurized gas transmission pipes. Kobayashi et al.[11,12] performed extensive experimental and numerical work in this area. This research showed that a physical constraint was able to arrest an axially propagating crack through the formation of flaps by the crack bifurcating into oppo-

site directions. While a monolithic line pipe is a much simpler structure than an aircraft fuselage, in the early 90's Kosai and Kobayashi[12] performed an analytical study applying the findings from the gas pipe studies to a full size aircraft fuselage with tear straps. In this study, a stationary axial crack in a stiffened, pressurized, cylindrical shell was studied using elastic and elastic-plastic analysis based on large deformation theory. The analysis predicted a large axial stress that preceded the crack tip and, based on the previously developed crack curving criterion, crack turning in much of the cylindrical shell. A comparison of the predicted axial stress to the circumferential stress in the vicinity of the crack tip was also made with the idea that crack turning occurred when the axial stress became larger than the circumferential stress. They additionally predicted that if the crack defeated the tear strap, the crack would continue to propagate in an axial direction.

Kosai et al.[13] expanded their research by performing analyses and experiments using laboratory scaled models of an ideal fuselage. For this study they used an elasto-dynamic finite element code to assess the effectiveness of the stiffeners. While this study included both circumferential and longitudinal stiffeners, one of the specimens was a cylindrical shell stiffened with tear straps which were twice as thick as the shell wall. The axial crack in this specimen propagated up to the tear straps and then followed the straps around the circumference.

During the same time Kosai et al.[12] studied this problem, Kanninen et al.[4] performed a static analysis of a stationary crack on a pressurized cylinder with tear straps. They concluded that the best approach for analyzing cracks with lengths greater than the tear strap spacing was using elastic-plastic geometrically nonlinear analysis.

1.4.1 Crack Turning Criteria

The mechanics behind the phenomenon of flapping and other forms of crack path instabilities have also been extensively studied and many theories have been developed. Some of the developed criteria include the maximum principal stress theory[14], the maximum hoop stress theory[14,15], the minimum strain energy density factor theory[16], and the maximum strain energy release rate theory.[17] All of the criteria predict the directional sta-

bility of a crack. These criteria are based on linear fracture mechanics and were developed for flat plates made from ideally brittle materials.

Two of the previously mentioned criteria are worth further discussion, the maximum principal stress criterion and the maximum hoop stress criterion. These criteria have two common traits. First, both are based on the hypothesis that a crack will propagate in the direction perpendicular to the greatest tension. Secondly, both are applicable only to the stresses near the crack tip. These criteria differ in that the maximum principal stress criterion, as implied by the name, employs the largest principal stress as the source of greatest tension. For the maximum hoop stress criterion, the source of tension is assumed to be the stress, in polar coordinates, normal to the vector connecting the crack tip and the point where the original stresses have been determined, see Fig. 1.4. Zaal[18] had some success in applying the maximum hoop stress criterion to cylinders and concludes by recommending this criterion for studying the directional stability of cracks.

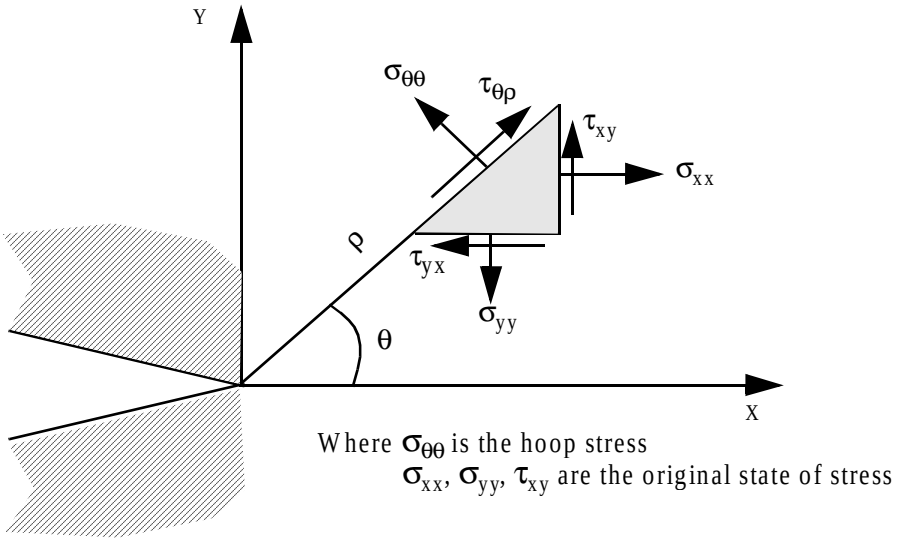

Fig. 1.4 Diagram of the hoop stress (the maximum hoop stress theory).

1.5 Objectives and Approach

This study concentrates on two objectives. First, we investigate the mechanics of ductile fracture on the path of an initially axial crack in an internally pressurized, aluminum cylindrical shell as the crack approaches an externally bonded tear strap. Secondly, the results

of the first objective are used to design a set of tear straps with various dimensions for experimental verification of the analytical results.

The approach is to first develop an analysis for the static, nonlinear response of the stiffened cylindrical shell using a ductile fracture criterion for crack growth. This analysis is performed using the finite element software STAGS (STructural Analysis of General Shells[19]). An experiment conducted at the NASA Langley Research Center is used to verify the finite element model. Using the verified model, a parametric study is conducted to investigate the influence of the size of a tear strap on the turning of the crack in the circumferential direction. In this parametric study, both the thickness and width of the tear strap are varied. The results of the parametric study are the basis for assessing the capability of the tear strap to deflect the crack, or not to deflect the crack, into the circumferential direction. These data of the influence of strap size on the fracture path are used to determine designs of new test articles.

CHAPTER 2

Fracture Test of a Pressurized, Stiffened Cylindrical Shell

2.1 Introduction

The problem of an axially propagating crack in the fuselage skin of the pressure cabin has been studied since the 1950's, but full scale fuselage testing is expensive. To understand the fundamental mechanics of fracture, laboratory scale models are used to obtain an understanding of the fundamental mechanics. The stiffened shell fracture test discussed in this chapter was performed at the NASA Langley Research Center, Structural Mechanics Branch, during the summer of 1997. It was this experiment which provided the motivation for this analytical study. A description of the laboratory scaled specimen, the subsequent test, and the test results are presented below.

2.2 Stiffened Cylindrical Shell Test Specimen

The specimen in the experiment was fabricated from an existing unstiffened, cylindrical shell with a two inch crack centered along the length. This shell was made from a 0.04-inch-thick, 2024-T3 bare aluminum alloy sheet which was rolled into a cylinder with a nine inch radius. The dimensions of the shell are shown in Fig. 2.1.

A double lap-joint splice configuration joined the edges of the sheet as shown in Detail A of Fig. 2.1. These 0.04-inch-thick splice plates, also fabricated from 2024-T3 bare aluminum, span the entire length of the specimen. Fifty-two rows of two 0.125 inch solid alu-

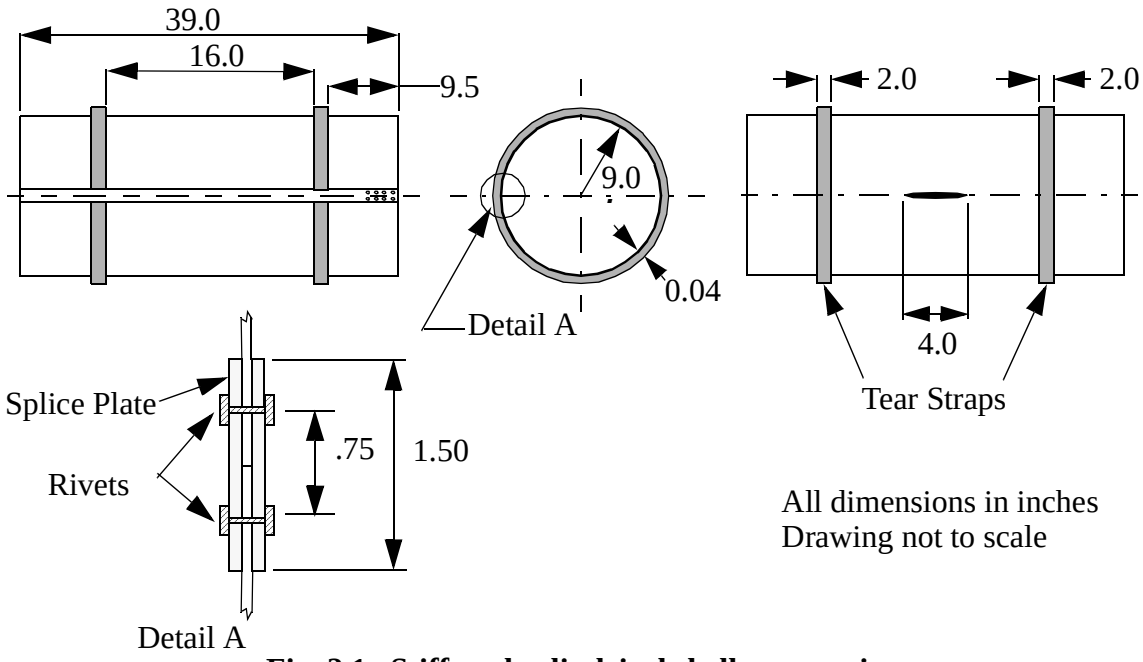

Fig. 2.1 Stiffened cylindrical shell test specimen.

minum rivets spaced 0.75 inches apart and EA-934 bonding paste adhesive secured the joint.

The two tear straps, 2.0 inches wide by 0.156 inches thick, were fabricated from 2024-T3 alclad. There was no scientific approach to the sizing of the tear straps. These dimensions were based on the available sizes of aluminum strips which were believed to be thick enough to induce flapping. Neither tear strap wrapped completely around the circumference of the cylindrical shell. Instead, the ends of the tear strap were flush against the splice plate. This eliminated the need for the tear straps to step over the splice plate. A 0.005 inch layer of the general aerospace epoxy FM73 was used to bond the tear straps to the exterior of the cylindrical shell. Ideally, the center line of each tear strap was to be placed 10.5 inches from the ends of the cylindrical shell and run circumferentially on the exterior except over the double lap-joint splice plate. Unfortunately, during assembly, the tear straps slipped, which resulted in a reduction in the distance between the tear straps from 16.0 inches to 15.875 inches. However, because of the small amount of slip, the spacing between the tear straps will be taken as 16.0 inches for the remainder of this study.

The existing shell had an axial crack two inches long located at the mid length of the shell, 180° away from the double lap-joint, and is also shown in Fig. 2.1. For this experiment with the tear straps, the crack was lengthened to four inches by wire electrical discharge machining using a 0.016 inch cutter. In addition, the tips of the crack were sharpened by hand with a razor blade.

2.3 Instrumentation

To monitor the behavior of the crack during pressurization, the stiffened shell was instrumented with one crack gage and 44 strain gages. For capturing the crack growth, the specimen was instrumented with a single crack propagation gage of type TK-09-CPC03-003/DP manufactured by Measurements Group, Inc. This type of crack gage consists of 20 foil grid lines on a glass-fiber reinforced epoxy matrix. As the crack propagates beneath the gage, the foil grid lines break and the electrical response is recorded. The gage was placed such that the first foil grid line was as close to one of the crack tips as possible. In this location, the gage captured approximately the initial 1.62 inches of crack growth.

To measure the strains in various locations on the cylindrical shell and tear straps, strain gages of type CEA-06-187UW-350, also manufactured by Measurements Groups, Inc., were used. These strain gages were located in 22 different positions on the specimen in back-to-back pairs, one gage on the interior wall and one on the exterior wall of the specimen. Each pair was positioned in either the axial or circumferential direction. The coordinate system for locating the strain gages is shown in Fig. 2.2. The actual location and direction of the strain gages are listed in Table 2.1 .

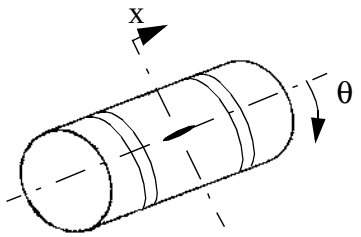

Fig. 2.2 Coordinate system.

Table 2.1 Strain gage locations and orientations.

Gage No.	x (in)	θ (degs)	Direction
1 & 2	2.0	0.0	circumferential
3 & 4	3.0	0.0	circumferential
5 & 6	2.0	5.0	circumferential
7 & 8	0.0	0.0	circumferential
9 & 10	0.0	5.0	circumferential
11 & 12	0.0	90.0	circumferential
13 & 14	0.0	270.0	circumferential
15 & 16	0.0	180.0	circumferential
17 & 18	0.0	0.0	axial
19 & 20	17.0	0.0	axial
21 & 22	9.0	0.0	circumferential
23 & 24	-9.0	0.0	circumferential
25 & 26	9.0	90.0	circumferential
27 & 28	9.0	270.0	circumferential
29 & 30	10.0	0.0	axial
31 & 32	8.0	0.0	axial
33 & 34	-8.0	0.0	axial
35 & 36	-10.0	0.0	axial
37 & 38	10.0	0.0	circumferential
39 & 40	8.0	8.0	circumferential
41 & 42	-8.0	0.0	circumferential
43 & 44	-10.0	0.0	circumferential

The specimen was also instrumented with four direct current differential transformers (DCDTs) and a pressure meter. The DCDTs measured displacements near the locations of the strain gage pair 11 and 12 and the gage pair 13 and 14. Another DCDT was placed on the double lap joint at the mid length of the cylinder. A fourth, located on an end cap, mea-

sured axial shortening or lengthening. Other details concerning the DCDTs as well as the pressure meter were not available at the time of this writing.

2.4 Sealing Features

A patch placed over the initial crack and potting the ends of the stiffened cylindrical shell into end caps served to seal the specimen and prevent pressure leakage. The patch was made from three 10 inch by 14 inch layers, an inner layer of 0.006 inch steel shim stock and two outer layers of a rubber-type material. With the 14 inch side parallel to the axial direction, the patch was centered on the crack. Before adhering the patch to the shell wall, the instrumentation leads were lead through the crack and into the interior of the stiffened cylinder. An RTV-type adhesive was used to create a seal between the leads, cylindrical shell, and the outer perimeter of the patch.

The two circular end caps were fabricated from 2024-T3 aluminum, each cap being two inches thick with a twenty-two inch radius. A circular groove 1.5 inches deep was machined around the center of each end cap to receive the ends of the cylindrical shell. See Fig. 2.3. An adhesive (3M Scotchweld 2216) was used to bond the ends of the cylin-

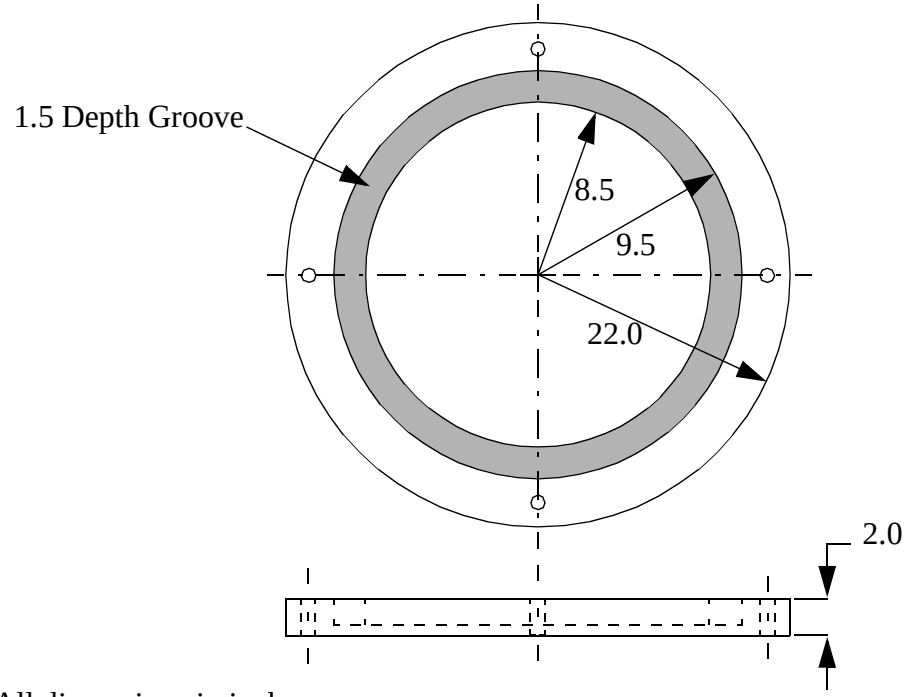

All dimensions in inches
Drawing not to scale

Fig. 2.3 General dimensions of the end caps.

drical shell in the grooves of the end caps. Four rods were used to contain the end caps in the event of an accidental failure of the bond. These rods were 43 inches long, spaced equally around circumference outside of the shell, and were inserted through holes drilled near the periphery of the end caps. Nuts were threaded on ends of the rods, but were not tightened against the end caps. One end cap contained a cut out for a trap door which allowed a location for the instrumentation leads to exit the specimen. This trap door was centered on the end cap and is twelve inches by ten inches. An O-ring around the perimeter of the door provides a seal between the end cap with the cut out and the trap door.

2.5 Test Equipment and Procedure

Testing of the specimen took place in a concrete bunker at the NASA Langley Research Center. All gages were calibrated and zeroed. For the test, the model was quickly pressurized to 15 psi with bottled air. After reaching 15 psi the pressurization rate was decreased, but not held at a constant rate. Because of the explosive nature of the experiment, viewing of the specimen was remote.

2.6 Experimental Results

During the experiment, stable crack growth was observed until an internal pressure of 46.52 psi was achieved. At this point, the crack growth became unstable and the specimen quickly failed. The tear straps were able to induce flapping as the crack deflected into the circumferential direction. The experiment did not damage the tear straps and the bond between the tear straps and the cylindrical shell remained intact. A photograph of the failed specimen is shown in Fig. 2.4.

Inspection of the failed specimen detailed the crack path. The initially axial crack propagated in a self similar manner until the crack tip was 0.23 inches away from the edge of the tear strap. At this point, the crack bifurcated into two unsymmetrical paths. Each path made gradual turns into the circumferential direction toward the tear strap. Then the paths followed the edge of the tear strap. The crack behavior was nearly identical for both crack tips encountering tear strap. This was expected since the specimen itself was sym-

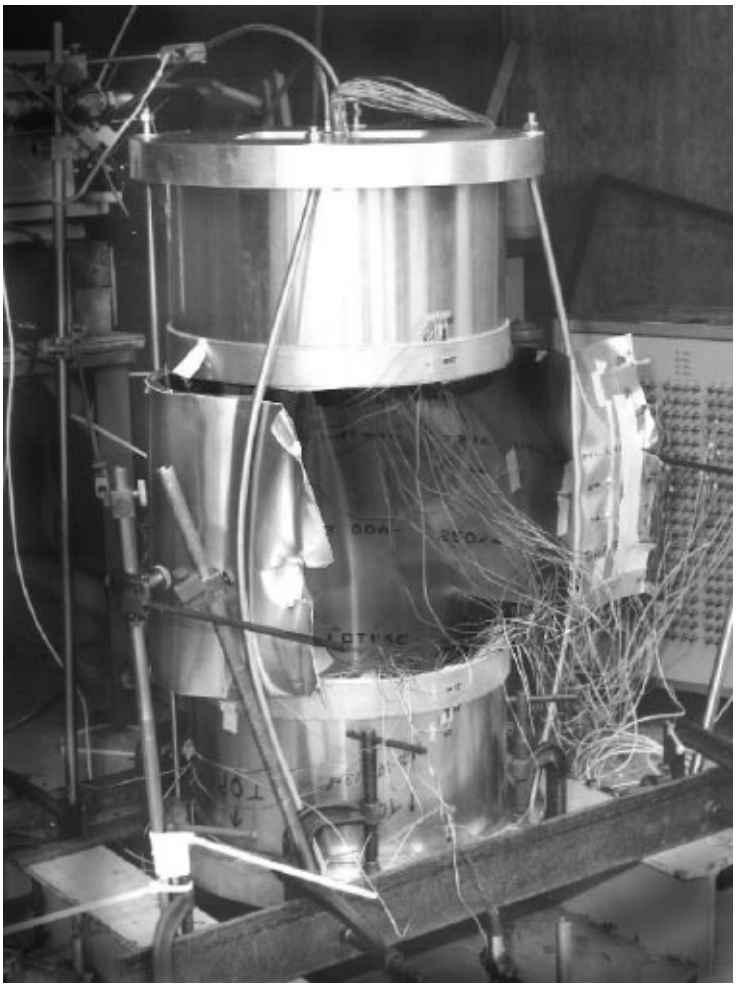

Fig. 2.4 Photograph of the failed stiffened cylindrical shell.

metric. A photograph of the location the crack bifurcation, turn, and the circumferential crack path is shown in Fig. 2.5.

Based on the data from the crack growth gage, the amount of stable crack growth was 0.56 inches. Since the test was pressure controlled, once the crack growth became unstable the crack immediately grew beyond the range of the crack growth gage. Meaningful data was not collected from the strain gages during the dynamic period of unstable crack growth.

Fig. 2.5 A Photograph of the surface of the failed specimen showing crack bifurcation, turns, and the circumferential paths.

2.7 Summary of the Experiment

The key results from the pressurized shell fracture test are as follows.

- For an initial axial crack length of 4.0 inches in the stiffened cylindrical shell, the maximum pressure during stable crack growth was 46.52 psi and the length of stable crack growth was 0.56 inches.
- The externally bonded tear strap, 0.156 inches thick by 2.0 inches wide, caused flapping by deflecting the axially propagating crack into the circumferential direction.
- At a distance of 0.23 inches before the edge of the strap, the crack bifurcated and the unsymmetrical paths gradually turned into the circumferential direction before running parallel to the tear strap.

These experimental results will be used to develop an analytical model in the finite element software STAGS. The following chapter presents the development and verification of this model.

CHAPTER 3

Stable Crack Growth and Correlation with Experiment

3.1 Introduction

This chapter addresses the mechanics of ductile fracture on the path of an initially axial crack in an internally pressurized, aluminum cylindrical shell as the crack approaches an externally bonded tear strap. Included in this chapter is a discussion of the features in the STAGS computer code that are important to this study, as well as a description of the analytical model and the process for correlating the analytical model using the experimental data.

3.2 The STructural Analysis of General Shells (STAGS) Code

The software used in this study is the structural analysis program STAGS (STructural Analysis of General Shells) version 3.0.[19] This software, developed in a joint effort between NASA and Lockheed-Martin, contains features that are specific for the general purpose analysis of arbitrarily shaped shells. STAGS is coded to produce load controlled solutions as well as solutions controlled by the Riks arc-length parameter technique. Other features of STAGS include linear static solutions, nonlinear static solutions using a true or modified Newton-Raphson procedure as well as a corotation procedure, buckling analysis, crack growth procedures, and the ability to incorporate user written subroutines. STAGS also accounts for material nonlinear behavior and geometric imperfections. Of these features, this study uses the Riks arc-length parameter technique in the solution for the geo-

metric nonlinear response, the true (or full) Newton-Raphson procedure, nonlinear elastic-plastic material behavior, and the crack growth algorithms. The remainder of this section will provide descriptions for the features of nonlinear material behavior and one of the crack growth procedures.

3.2.1 Nonlinear Material Behavior

The model of metal plasticity used in the STAGS code is the White-Besseling theory, which is also called the overlay model or multiple subvolume model.[20] This material model represents the material behavior with a number of elastic-plastic components linked in parallel. As load is applied to the material, equal strains are introduced into each elastic-plastic component. However, each elastic-plastic element has a different value of yield. This results in a piecewise linear approximation for the stress-strain behavior of the material.

The user can specify up to ten points on the stress-strain curve not including the origin, where the origin is assumed to be the point of zero stress and strain. The slope between the origin and the first user defined point must correspond to elastic material behavior and the remaining points must be defined such that the slope of each successive segment decreases. If the strain in an analysis exceeds the largest user defined strain, perfectly plastic material behavior is assumed.

3.2.2 Stable Crack Growth Algorithm

One of the crack growth algorithms in STAGS calculates equilibrium configurations of the shell for stable crack growth, or slow crack growth. An example plot of a stable crack growth curve, which is a plot of the applied load versus crack length, is shown in Fig. 3.1. Each point on the crack growth curve corresponds to an equilibrium configuration of the shell at a given pressure and crack length. Stable crack growth is characterized by the portion of the

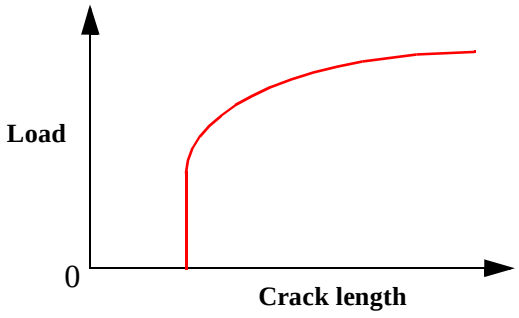

Fig. 3.1 Stable crack growth curve.

crack growth curve with a positive slope. An increase in load is required to advance the crack.

The STAGS code is not programmed to calculate the direction of crack growth, which involves the difficult issue of stability of the path for a curved crack or kinked crack under ductile fracture. Hence, the user defines not only the initial crack, but the path the crack will follow as the crack extends. Prediction of crack extension in a metal requires a ductile fracture criterion, and the criterion we used in STAGS is based on the crack tip opening angle, or CTOA. The crack tip opening angle is the angle between the open faces of a crack measured in the tangent plane to the reference surface in the deformed configuration. For a finite element model the dimensional parameters to compute the CTOA are shown in Fig. 3.2, and the equation for the CTOA is

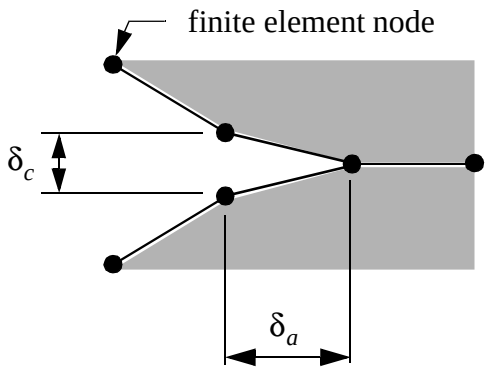

Fig. 3.2 Dimensions for the CTOA.

$$\text{CTOA} = 2\tan^{-1}(\delta_c/(2\delta_a)) \tag{3.1}$$

Crack growth is predicted by a specified value of the critical crack tip opening angle[21, 22] ($CTOA_c$). Using the $CTOA_c$, equilibrium points for stable tearing of a user defined crack are computed through a nodal release technique called load relaxation.[6]

The process of load relaxation allows equilibrium to be established as the crack advances a distance (δ_a) equal to the amount of separation between two adjacent nodes. The nodal release technique is illustrated in Fig. 3.3. Along the user defined crack, each node is actually two nodes, a master and slave node. At locations where the crack is closed, the master and slave nodes are constrained to be dependent. For locations where the crack is open, the nodes are independent of each other unless the crack is defined to propagate along a line of symmetry. If the crack path is along a line of symmetry, the construct of the master-slave node pair is not necessary since the node released on the line of symmetry has an image node inferred by conditions of symmetry. Consequently, the plane

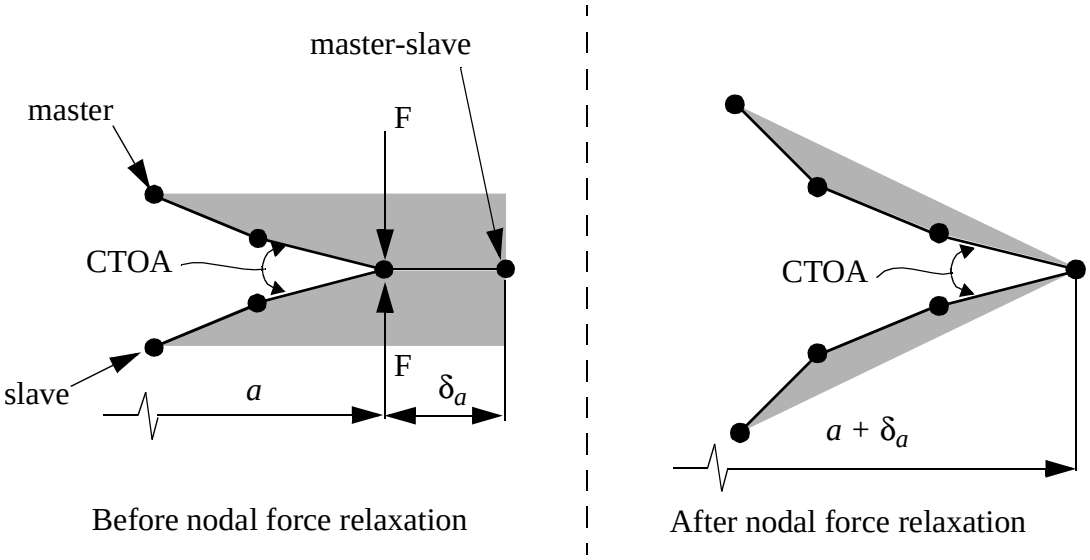

Fig. 3.3 The nodal release technique in load relaxation.

of symmetry and the displacements of the released node and the new crack tip node are sufficient to determine the CTOA.

The CTOA is calculated for every increase in pressure. Once the calculated CTOA becomes within 5% of the $CTOA_c$, the pair of crack nodes is released at the crack tip. At this point, as shown in the left side of Fig. 3.3, the master and slave nodes are held together by the nodal force *F*. Decreasing the magnitude of this force immediately to zero for the longer crack length often results in divergence of the Newton's solver for the new equilibrium state. Instead, the load relaxation algorithm fixes the applied pressure load and then decrements the nodal force *F* so that the Newton's solver converges to an equilibrium state for each succeeding smaller value of *F* until *F* vanishes, as is indicated in the sketch in the right side of Fig. 3.3. With the load relaxation complete and equilibrium established for the model with the longer crack length, the CTOA is calculated with the new crack tip and, provided the calculated CTOA is not within 5% of the $CTOA_c$, the process of increasing the pressure applied to the model resumes.

3.3 Finite Element Model of the Pressurized Shell

Development of the finite element model for this study is focused in two areas, physical features and the choice of mesh. The physical features of the finite element model for this

study are based on the experimental specimen. The mesh is controlled by the type of elements available in STAGS as well as keeping the total number of elements to a minimum.

3.3.1 Model Features

Producing the smallest analytical model requires taking advantage of the symmetry of the experimental specimen. Since the experimental specimen has two planes of symmetry, only one quarter of the specimen is modeled. The basic model consists of a perfect cylindrical shell and a tear strap with dimensions identical to the experimental specimen shown in Figure 2.1 on page 10, and listed in Table 3.1. The double lap joint in the cylindrical

Table 3.1 Model data.

Cylindrical Shell		Tear Strap	
Inside Radius	9.00 inches	Inside Radius	9.00 inches
Thickness	0.04 inches	Thickness	0.156 inches
Half Length	19.50 inches	Width	2.00 inches

shell of the experimental specimen is not included in the analytical model. Since the crack is on the opposite side of the shell as the double lap joint and tear strap edge, 180° away from the center of the double lap joint, it is assumed the double lap joint and discontinuous tear strap does not effect the behavior of the propagating crack or the stress field surrounding the crack. Without the presence of the double lap joint, the tear strap becomes a continuous ring around the cylinder.

Symmetry boundary conditions apply to the three edges which lie along the lines determined by $x = 0$ inches, $\theta = 0°$, and $\theta = 180°$. The initial longitudinal crack is located on the $\theta = 0°$ line of symmetry with a half length of two inches. The end caps at $x = 19.50$ inches are not modeled in the analysis and their effect is represented by idealized end conditons. The boundary conditions for the fourth edge at $x = 19.50$ inches are that all degrees of freedom are specified to be zero except for the axial displacement. Instead of specifying the axial displacement at the $x = 19.50$ inches, the axial line load is specified to be spatially uniform around the circumference with a magnitude equal to one-half the pressure

times the radius. Since the crack path is not to be specified in the portion of the model between the tear strap and the potted end, it is assumed the effects of the simplified boundary conditions at x = 19.50 inches are negligible on the shell response in the vicinity of the crack path.

The material properties for 2024-T3 aluminum are used for both the shell wall and the tear strap. The linear elastic properties for the 2024-T3 AL are listed in Table 3.2, and the piecewise linear approximation to the nonlinear strain-stress curve is listed in Table 3.3. These material properties were experimentally determined by Dr. Jim Newman of the Fracture Mechanics Branch at the NASA Langley Research Center.

Table 3.2 Elastic material properties of 2024-T3 AL.

Young's Modulus	10.359×10^6 psi
Poisson's Ratio	0.3
Specific weight	0.101 lb./in^3

Table 3.3 Nonlinear strain-stress data for 2024-T3 AL.

Strain (ε)	Stress (σ), psi
0.00483	50.0365×10^3
0.01500	56.5627×10^3
0.04000	62.3640×10^3
0.10000	68.1653×10^3
0.16000	71.0660×10^3
1.00000	72.5163×10^3

Accounting for the internal pressure, a dead load or a live load (hydrostatic pressure load) can be specified. In a geometrically nonlinear analysis, a hydrostatic pressure is usually used. A comparison of an analysis which uses a live load against an analysis which

uses a dead load shows the two types of loading produces approximately the same results. This is because the geometric nonlinearity in this study is confined to the vicinity of the crack. Therefore, a dead load which acts on the inside diameter of the entire model and is directed outward in the radial direction is used. In a nonlinear analysis in STAGS, loads are applied gradually in load steps. Proportional loading is assumed and the applied loads are specified by a load factor. In this study, an applied load factor of 1.0 corresponds to an internal pressure of 46.52 psi, the maximum experimental pressure, and an axial stress resultant of 209.34 lb./in at x = 19.50 inches.

3.3.2 Elements and Mesh Refinement

Two general types of elements are used in this model. Of the elements in the STAGS element library, the E410 element is the best to use for thin walled structures such as the stiffened cylindrical shell of this study.[19] This element is a simple four node quadrilateral plate element with a cubic lateral displacement field and six degrees of freedom per node. STAGS also contains specialized elements to allow a transition from a coarser to a finer mesh. This type of specialized element is the 510 or 710 transition element. A more in depth discussion of the transition element is found in the STAGS User Manual[19] but a brief description is provided here. Basically, these elements are five or seven node elements with six degrees of freedom per node. These elements impose an edge compatibility between the boundaries where the mesh size doubles. The 510 transition elements are used where one edge of the element is along a boundary where the mesh doubles. The 710 transition elements is used for elements which have two boundaries where the mesh doubles. Based on how the user defines the boundaries, STAGS automatically chooses which transition element to use in place of a E410 element.

Element size varies throughout the entire model to keep the number of elements in the model to a minimum. The finest of mesh refinement is located around the area surrounding the user defined crack path. These elements have an aspect ratio of approximately one as the nodes are spaced 0.08 inch apart. This small element size is necessary to accurately calculate the CTOA and predict the yielding at the crack tip.[23] Moving away from the crack area, the spacing between the nodes increases and the aspect ratio does not always

remain one. The largest elements are located at θ = 180° and *x* = 19.50 inches, where the boundary conditions and axial load are applied. A typical mesh for the model of the experimental specimen is shown in Fig. 3.4. The self similar crack growth model contains 4,400 elements and has approximately 30,000 degrees of freedom.

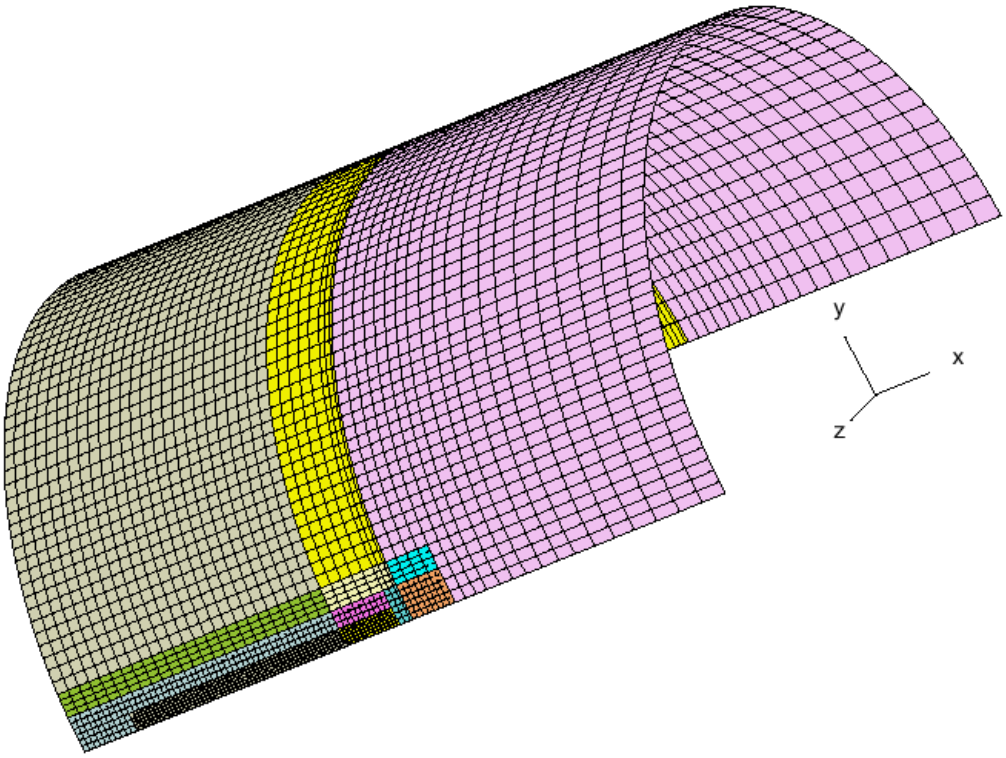

Fig. 3.4 Typical finite element mesh to model the test specimen.

3.4 Model Correlation With Experimental Stable Crack Growth Results

To complete the analytical model based on the experiment, a crack needs to be added to the previously described model shown in Fig. 3.4. The analytical model must include an axial crack with an initial half length of two inches which is located on the θ = 0° line. Since correlation of the analytical model with the experimental results only concerns stable crack growth and the stable crack growth during the experiment was self similar, the crack path in the model is also self similar. For correlating the model, the specified crack path only needs to extend slightly beyond the amount of stable crack growth in the experiment. Therefore, the specified crack path is axial with an initial half length of 2.00 inches and a final half length of 2.72 inches.

3.4.1 Solution Procedure

The model is analyzed using a nonlinear static analysis. The analysis uses the Vector Space Solver for the solution of the nonlinear equations.[24] Initially, the solution is determined under load control, however, after a few load steps have been solved, the solution control strategy changes to the Riks arc-length control. To avoid convergence problems, a true, or full, Newton's Method is used. An example of a solution input file is given in Appendix A. A SUN Enterprise 4500 with two Ultra Sparc II 400MHz processors and 1 gigabyte of memory is the NASA computer used for most of the analyses in this study.

3.4.2 $CTOA_c$ Selection

Unfortunately, the $CTOA_c$ is not a material constant as it is dependent on mesh size, type of element, and material thickness.[22] A parametric study varying the value of the $CTOA_c$ is used to determine a value for which the analytical model is correlated with the results of the experiment discussed in Chapter 2. Correlating the analytical results with the experimental results requires matching the quantities of the maximum pressure achieved during stable crack growth (fast crack pressure), the amount of stable crack growth, and the far field circumferential strains during stable crack growth.

An initial $CTOA_c$ angle of 5.36° was obtained from a published study by Starnes and Rose.[23] This $CTOA_c$ produces a maximum stable crack growth pressure of 52.10 psi, which is 12% greater than the experimental maximum pressure, but with an exact amount of stable crack growth, 0.56 inches. An incorrect maximum pressure is expected since the study by Starnes and Rose[23] used elements 0.04 inches in width along the crack and this study uses elements twice as wide. Learning from these initial results, the $CTOA_c$ is gradually decreased to a value of 5.00°. The lower $CTOA_c$ drops the maximum pressure to 47.66 psi, which is only 2.5% greater than the experimental result. This value of the $CTOA_c$ does increase the amount of stable crack growth by 0.08 inches to 0.64 inches. However, considering the error in the crack growth gage and the 5% tolerance in matching the $CTOA_c$ in STAGS, the difference between the two results is acceptable. The crack

growth curves, internal pressure versus half crack length, during stable crack growth from the experiment and the analysis are shown for comparison in Fig. 3.5.

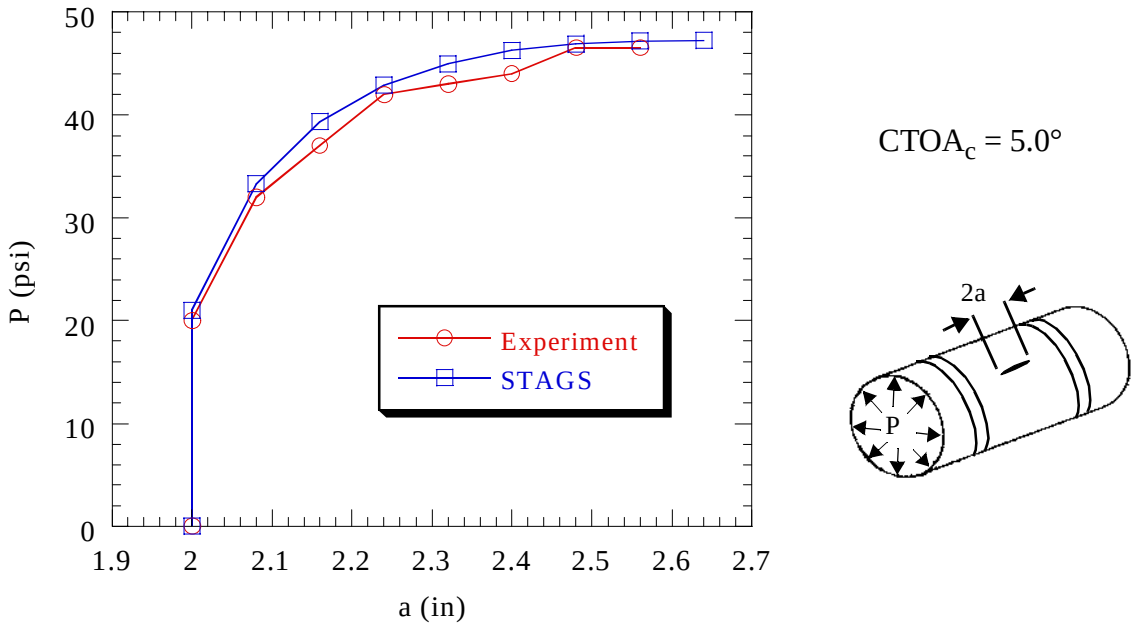

Fig. 3.5 Stable crack growth curves.

In this study, the prediction of the pressure for the initiation of stable crack growth is not considered. This value is difficult to predict because the initial amount of crack extension, less than the thickness of the material, is a transition area. Throughout the transition area, the CTOA is not a constant value due to phenomena such as crack tunneling and transitions from flat-to-slant fracture.[21] These phenomena make it difficult to obtain a true crack initiation pressure since crack gages, like the one used in the experiment, can not measure these effects. The first crack gage wire could have also failed before the crack actually began to grow. Considerable error also comes from the geometry of the crack tip as it is impossible to have a crack in an experimental specimen with an infinitely sharp crack tip. To handle the initiation of crack growth, a different value for the CTOA$_c$ is used in STAGS for the release of the first pair of crack nodes. From trial and error, it appears that a CTOA$_c$ of 2.8° will yield an analytical crack initiation pressure within 5% of the experimental pressure of 20 psi.

Of the 44 strain gages on the experimental specimen, only four measured far field strains. These four, gages 11-14 located in the center of the experimental model ±90° from the crack, measured the internal and external circumferential strains. A plot of the pressure as a function of the experimental strains reveals both membrane and bending strains as the internal gages shows a larger strain than their corresponding external gages. Since the bending strain is due to the double lap-joint splice configuration, which is not included in the analytical model, the internal and external strains of the experimental results are averaged to remove the bending component from these strains. The averaged experimental strains are compared to the analytical results. A comparison of the experimental and analytical strain results to the strength of materials results which is from can also be made. The circumferential strain from a strength of materials is[25]

$$\varepsilon_c = (\Delta R)/R = [(1-\nu/2)PR^2]/(ERt) \tag{3.2}$$

Excellent correlation between the experimental strain, analytical strain, and the strength of material result is shown in Fig. 3.6. This confirms the choice of a $CTOA_c$ of 5.0°.

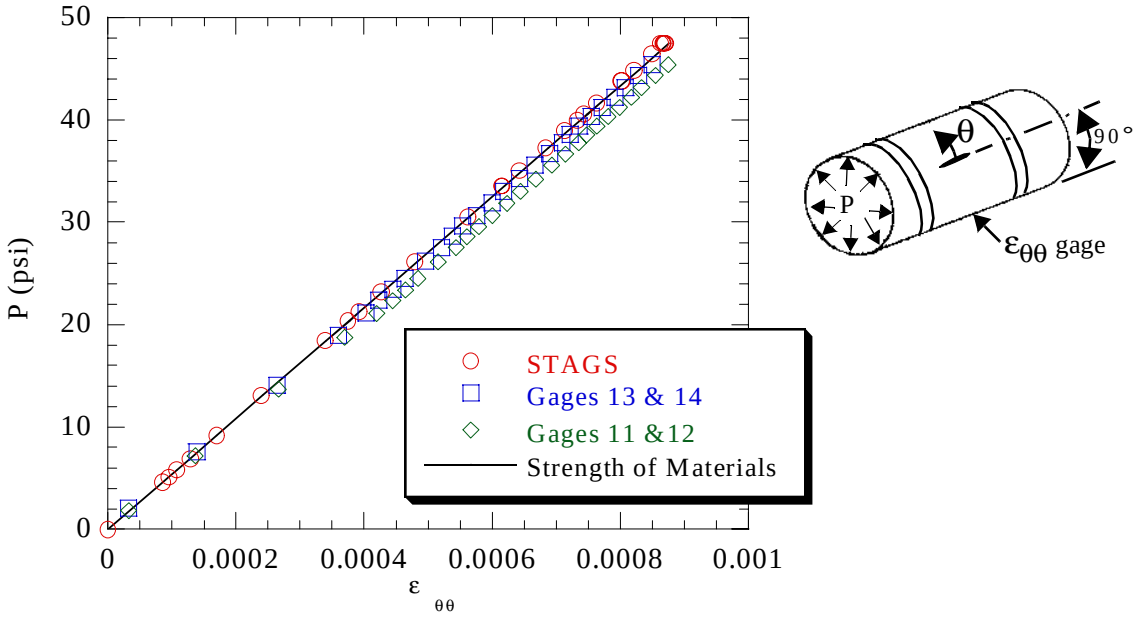

Fig. 3.6 Far field strains during stable crack growth.

With verification of the analytical model through the selected $CTOA_c$ of 5.0°, the next step is to begin the static nonlinear analysis of the model that allows the crack to approach and defeat the tear strap. This is the focus of the next chapter.

CHAPTER 4

The Unstable Portion of the Self Similar Crack Growth Path

The previous chapter concluded with the determination of a $CTOA_c$ which correlated the analytical model with the experimental results. Next, the analytical model and solution file is modified in order to study the behavior of a crack as it approaches the tear strap. The major issue addressed in this chapter is self similar crack growth of the axial crack through the unstable portion of the crack growth curve and into the toughened structure at the tear strap. While the stable crack growth algorithm is able to produce equilibrium points during regions of unstable crack growth, the results are not particularly useful as the algorithm can not decrease the pressure. Clearly, the numerical algorithm for stable crack growth in the STAGS code is not amenable for the analysis through the unstable portion of the crack growth curve. Fortunately, the code is programmed with an alternative algorithm to establish static equilibrium states on the unstable portion of the path.

4.1 Self Similar Crack Growth Model

Recall that in the experiment the crack path followed the $\theta = 0°$ line until the crack reached a half crack length of 7.77 inches. The crack propagates in a slow growth manner, corresponding to the stable portion of the crack growth curve, until a half crack length of 2.56 inches at a relative maximum pressure of 46.52 psi is reached. At the relative maximum pressure, fast crack growth commences and the axial path extends to the point of bifurcation at a half length of 7.77 inches. Consequently, the majority of crack propagation

in the experiment is self similar, and the fast crack growth implies that there are no stable static equilibrium states along a portion of the axial path from a half length of 2.56 inches to 7.77 inches.

An axial crack path on the $\theta = 0°$ line initiating from a half length of 2.0 inches to a final half length of 8.72 inches is specified in the STAGS model. The final half crack length of 8.72 inches is near the middle of the tear strap width. A perfect bond between the shell wall and tear strap is assumed. Hence, as the crack propagates through the tear strap, the crack defeats both the shell wall and the tear strap in the analysis. Also, it is assumed the $CTOA_c$ remains 5.0° even after the crack moves into the tear strap. The reason for this assumption is because it is not known exactly how the $CTOA_c$ will behave after entering the tear strap. The mesh for this model is identical to the mesh which is used to correlate the model.The mesh with the initial axial crack and the self similar crack growth path is shown in Fig. 4.1. An example of the input file for this model can be found in Appendix A.

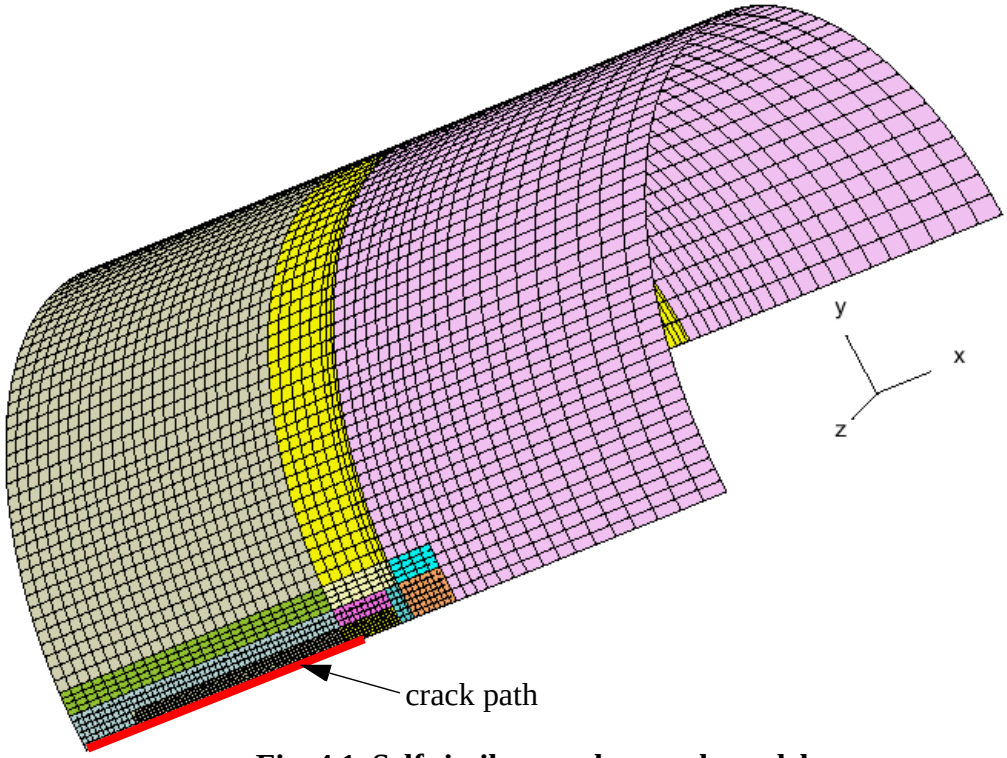

Fig. 4.1 Self similar crack growth model.

4.2 Unstable Crack Growth Algorithm

Since it is desired to advance the crack up to and eventually through the tear strap, the analysis must extend the crack not only through the region of stable growth, but also through the region of unstable crack growth. The demarcation of the crack growth curve into stable and unstable segments is defined by horizontal slopes, at which the load may take on extremum values. An example of the division of the path from stable to unstable states occurring at a relative maximum load is shown in Fig. 4.2. The initial portion of the curve, which was discussed in the previous chapter, represents stable crack growth. Once the maximum load is achieved, the crack growth becomes unstable. This is characterized by the portion of the crack growth curve with a negative slope. Advancing the crack through equilibrium states along this portion of the curve can only be established by decreasing the applied load. When the load is the internal pressure, and it can only increase monotonically (as is the case in the experiment), the unstable static states cannot be observed in the laboratory. The consequence of onset of unstable crack growth in a structure is usually a rapid, catastrophic failure of the structure.

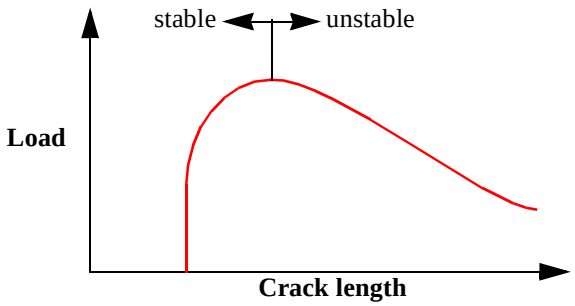

Fig. 4.2 Complete crack growth curve.

A new crack growth feature included in STAGS version 3.0 allows the calculation of equilibrium states in the region of unstable crack propagation.[26] This unstable tearing algorithm comes into play in STAGS if the calculated CTOA is violated immediately following the completion of a stable tearing load relaxation procedure. At this point of violation of the fracture criterion, the stable algorithm fails to converged since the applied load must decrease to establish equilibrium. A schematic of advancing the crack length in the unstable portion of the crack growth curve is shown in Fig. 4.3.

When the CTOA is immediately critical, the pressure applied to the model is not held to a constant value. Instead, the unstable algorithm is invoked in the code which adds a constraint equation that the CTOA is held fixed at its critical value as shown in the left

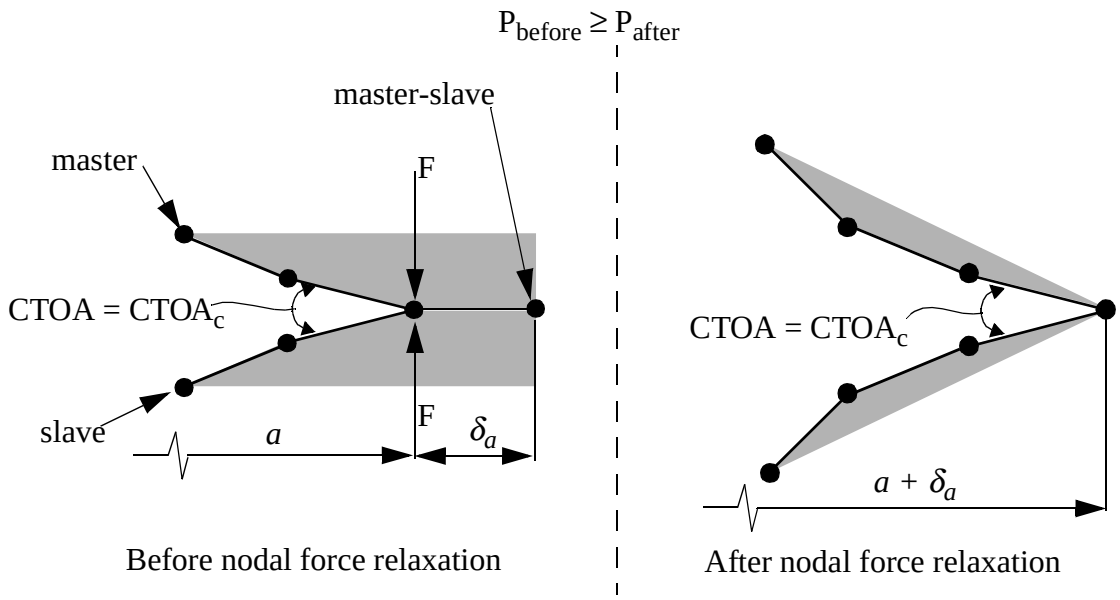

Fig. 4.3 Advancing the crack tip in the unstable portion of the crack growth algorithm.

side of Fig. 4.3. Both the applied load factor and the load relaxation factor become unknown. A nonlinear solution procedure is implemented to find the applied load factor at the completion of the load relaxation procedure such that the additional constraint on the CTOA is satisfied. Determination the applied load factor for the new crack length with the CTOA constrained to its critical value and the nodal force reduced to zero is illustrated in the right side of Fig. 4.3. With the load relaxation complete, the new crack tip node is released, and the unstable algorithm is repeated provided the CTOA calculated at the new crack tip is greater than the critical value. If the CTOA is less than the critical value, STAGS continues the solution by increasing the pressure applied to the model until the calculated CTOA exceeds the critical value.

4.3 Results of Self Similar Crack Growth

Two solution files are used for analyzing the self similar crack growth model. The first uses the exact solution file as for correlating the model. This particular solution file only calls the stable crack growth algorithm. The second analysis uses a modified version of the solution file for model correlation. Both the stable and unstable crack growth algorithms

are called by the modified solution file. An example of the STAGS solution file which calls both crack growth algorithms is shown in Appendix A.

The resulting crack growth curves are shown in Fig. 4.4. The difference in the result-

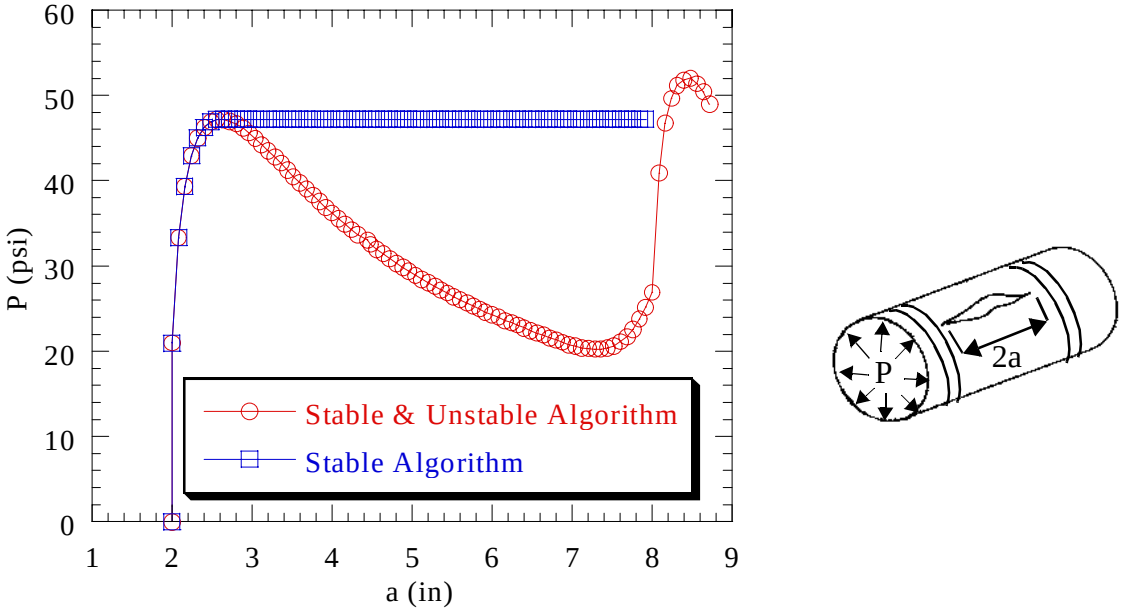

Fig. 4.4 Self similar crack growth curves calculated from the stable and unstable algorithms.

ing crack growth curves computed from the stable and unstable algorithms is clearly shown in this figure. During the initial 0.64 inches of stable crack growth the analyses are identical. It is past the region of stable crack growth where the curves dramatically differ. These curves also show that the majority of the crack growth through the model is unstable.

Once unstable crack growth begins, an analysis that uses only the stable crack growth algorithm produces a perfect horizontal line as shown in Fig. 4.4. This is due to STAGS keeping the pressure applied to the model constant while performing a load relaxation procedure as explained in the previous chapter. Each point on the horizontal portion of the curve is in equilibrium. However, these points are not realizable because at all of these points the calculated CTOA exceeds the $CTOA_c$.

Only using the stable crack growth algorithm also produces a curve that is identical to a crack growth curve from an experiment. This is because, similar to the stable crack growth algorithm, the experimental specimen can not depressurize due to the three layered patch which kept the model sealed for most of the crack growth. Even without a seal the experimental pressure would have remained a constant value because the rate of depressurization of the specimen is much slower than the rate of crack growth. During this situation of unstable or dynamic crack growth, the internal pressure can not decrease fast enough to allow the crack growth to be affected by the decrease in internal pressure.

The behavior of the crack as it moves through the tear strap using only the stable crack growth algorithm is not known, because convergence difficulties are encountered when the path moves into the strap. Hence, the analysis is terminated at a half crack length of 8.00 inches. It is believed that the analysis would continue to increase the pressure applied to the model once the half crack length reaches 8.16 inches. At this point both of the curves in Fig. 4.4 should coalesce until the crack growth through the tear strap becomes unstable.

Focusing on the curve resulting from using a combination of the stable and unstable crack growth algorithms, a different picture of the behavior of the crack as it approaches the tear strap is obtained. This crack growth curve shows the pressure decreasing from the relative maximum pressure at a half crack length of 2.64 inches, until the half crack length becomes 7.28 inches. At the half crack length of 7.28 inches the pressure reaches a minimum of 20.24 psi. After this point, the toughening effect of the tear strap can be seen on the behavior of the crack as an increase in pressure is necessary to further advance the crack. Advancing the crack into the tear strap requires yet even more pressure. This increasing pressure is necessary until the crack travels 0.48 inches into the tear strap. At this point the crack growth becomes unstable and the unstable crack growth algorithm continues to find equilibrium points where the $CTOA_c$ is not violated.

4.4 Discussion

The self similar crack growth model is able to produce an interesting result when used in conjunction with the unstable crack growth algorithm. From these initial analytical results, it is concluded that self similar crack growth through the tear strap is unlikely. The reason for this conclusion is that the pressure required to advance the crack beyond the first 0.16 inches of the tear strap is greater than the maximum pressure achieved during stable crack growth. Since the pressure can not change instantaneously during unstable crack growth, it remains equal to the maximum pressure of stable crack growth. The higher pressure required to push the crack completely through the tear strap is not available.

Unfortunately, these results do not conclusively establish that bifurcation of the path at a half crack length of 7.77 inches will occur. The crack could arrest at the strap rather than bifurcate and turn. The crack growth curve only shows that the toughening due to tear strap manifests itself at a half crack length of 7.28 inches. It is assumed from this result that the location of bifurcation, if it occurs in an analysis, will be at a half crack length greater than 7.28 inches. Since the results do suggest that the self similar crack growth path into the strap is unlikely, further analysis of crack path bifurcation is required. This will be the subject of the ensuing chapter.

CHAPTER 5

Crack Turning Model and Parametric Study of Various Tear Straps

5.1 Introduction

The self similar crack growth model and the ensuing results, shown in the previous chapter, indicate that the tear strap would arrest the crack if it followed a self similar path through the strap. In order to continue crack growth, the crack must turn into the circumferential direction before encountering the tear strap. This turning crack path more closely resembles the crack path formed in the experiment and is incorporated into the analytical model. The subject of this chapter is the development of a crack turning model and the subsequent results. After the development of a crack turning model, the results of a parametric study of various sizes of tear straps are presented.

5.2 Crack Turning Model

The actual path taken by the crack in the experiment is more complex than simple self similar crack growth. As discussed in Chapter 2, the crack initially propagates self similarly until the half crack length reaches 7.77 inches. At this point the crack bifurcates, and the two unsymmetrical branches turn into opposite circumferential directions running parallel to the strap.

This exact crack path is not incorporated into an analytical model for two reasons. First, it would be a challenging task to incorporate such a complex crack path into a STAGS input file. Crack path definitions in STAGS must follow the element boundaries,

meaning the crack path can not be defined to cut through an element. This eliminates the possibility of creating a smooth continuous curve as generated in the experiment. Since the size of the elements is small in the vicinity of the crack, the crack path could be approximated by following the element edges. However, specifying this type of crack definition in STAGS would require extensive input and would be extremely taxing. The second reason is that STAGS requires a crack path to be defined a priori. In addition, the crack path from the experiment is not expected to be correct for stiffened cylinders with different tear strap dimensions. This would require knowledge of the specific crack path for each tear strap geometry analyzed. Since the exact crack paths for stiffened cylinders with various tear strap dimensions are not known, a separate path directional stability analysis using other methods would be required to determine analytically the crack path. This extra analysis is beyond the scope of the present study, and would be a considerable undertaking in itself.

Instead of using the exact crack path, the simplest finite element modeling for crack bifurcation consists of defining bifurcated paths in the circumferential direction along element boundaries. Hence, the bifurcated paths are symmetric with respect to the axial path and the turn at the bifurcation point is ninety degrees. Clearly, this definition of the crack path cannot exactly capture what is observed in the experiment. However, it does provide an approximate path which more resembles the exact path and is not specific to any one tear strap size.

In five separate models, circumferential crack paths are modeled at the half crack lengths of 8.00 inches, 7.92 inches, 7.84 inches, 7.76 inches, and 7.68 inches. These turning locations are chosen such that the ninety degree turn occurs both before and after the location of crack bifurcation in the experimental specimen.

Defining a crack path that propagates in two different directions is more complicated than a single self similar crack growth path. Two different crack definitions, one which propagates the crack in the axial direction and a second which propagates the crack in the circumferential direction, delineates the crack that turns. The crack turning model is a modified version of the self similar crack growth model. Like the self similar crack growth

model, the crack turning model assumes a perfect bond between the cylindrical shell and tear strap. The major difference between the two models is in the section of the model where the crack path deviates from self similar crack growth. To allow the crack to propagate circumferentially a total of 0.94 inches, additional mesh refinement near the tear strap is necessary to maintain the 0.08 by 0.08 inch element size. The mesh refinement for the crack turning models and an example of a crack path are shown in Fig. 5.1. Appendix A contains one of the input files that involves crack turning. However, a brief description of the input for the crack turning model is provided here.

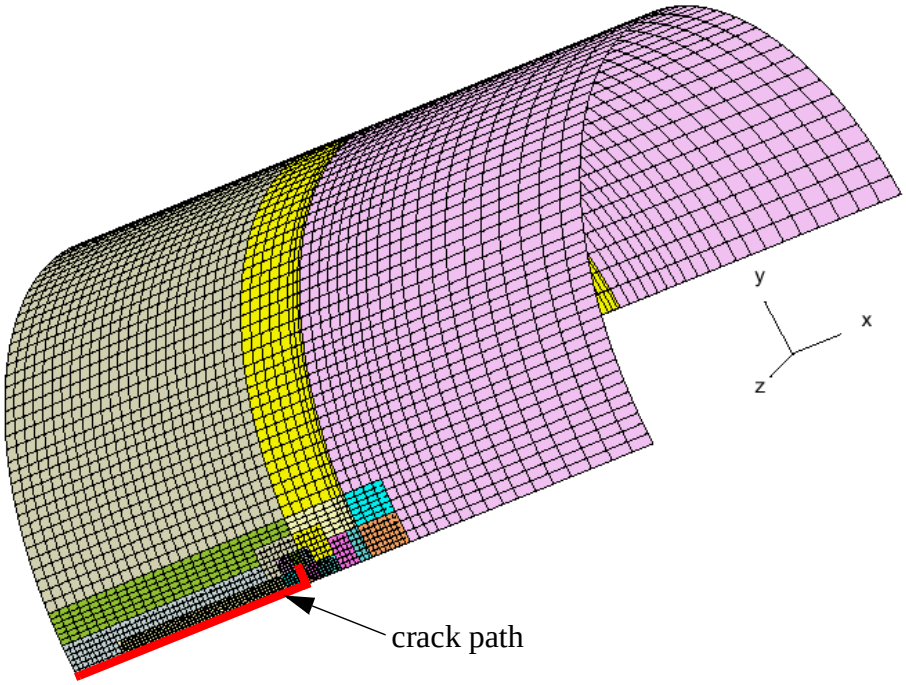

Fig. 5.1 Crack turning model.

The first part of the crack definition is the self similar portion of the crack which propagates along the $\theta = 0°$ line. Along the length of this portion of the crack, unrestrained boundary conditions replace the symmetry boundary conditions, and a special procedure is used to compute the correct CTOA. For correct calculation of the CTOA, nodes with symmetric boundary conditions are placed in the same location as the existing nodes along the length of the crack, $\theta = 0°$. The added nodes become the master nodes and the original nodes are the slave nodes in the master-slave relationship of a user defined crack. All of the master and slave nodes, where the crack is defined as closed, are constrained such that

all of the degrees of freedom are identical. Open master and slave nodes in the crack path are constrained to have identical axial and radial positions to ensure proper calculation of the CTOA. Given these crack definitions, the CTOA is now measured between the open crack face and the line of symmetry. Since only half of the angle between the two crack faces is measured, the $CTOA_c$ becomes 2.5°.

The second part of the crack definition describes the crack path in the circumferential direction. For this part of the crack it is important that the first pair of master and slave nodes are defined as open and their degrees of freedom are completely independent of each other. This open pair of nodes is necessary because STAGS needs a crack tip to calculate a CTOA before it can initiate crack growth. Since this pair of nodes is also included in the axial crack, the circumferential crack will not propagate until the axial crack opens completely. Because the actual behavior of the $CTOA_c$ as the crack propagates in the circumferential direction is unknown, the $CTOA_c$ for the second part of the crack definition is assumed to remain the full 5.0°.

Because the complete crack path is now defined through a combination of two cracks, there are two crack tips in the model. Unfortunately, the unstable crack growth algorithm is not programmed to handle a model with multiple crack tips. Without the capability of using the unstable algorithm, the analysis can only rely on the stable crack growth algorithm. This requires the model to have an initial half crack length greater than two inches. The reason for the longer initial half crack length is due to the fact that the stable crack growth algorithm can not decrease the pressure applied to the model during a node relaxation as shown in the previous chapter. Without decreasing the pressure from the first relative maximum pressure on the crack growth curve, the complete axial path to the bifurcation point cannot be modeled in the analysis. The resulting crack growth curve would be a horizontal line exactly as shown beforehand in Fig. 4.4. Unfortunately, changing the initial half crack length changes the resulting crack growth curve. Longer initial half crack lengths reduce the maximum pressure necessary to initiate unstable crack growth.[23] A comparison of the effect of the initial half crack length on the crack growth curve is constructed using initial half crack lengths of two and six inches. The difference

between the two crack growth curves can be significant, as shown in Fig. 5.2. However, the curves begin to merge after both curves have grown for more than about one inch. In fact, once the crack enters the tear strap (a > 8.0 inches) the two curves appear to completely merge. Since the two curves agree reasonably well at the locations of crack turning, the initial half crack length of six inches is used in all of the crack turning models. Using the smaller initial half crack length also has the major advantage of cutting the computation time in half.

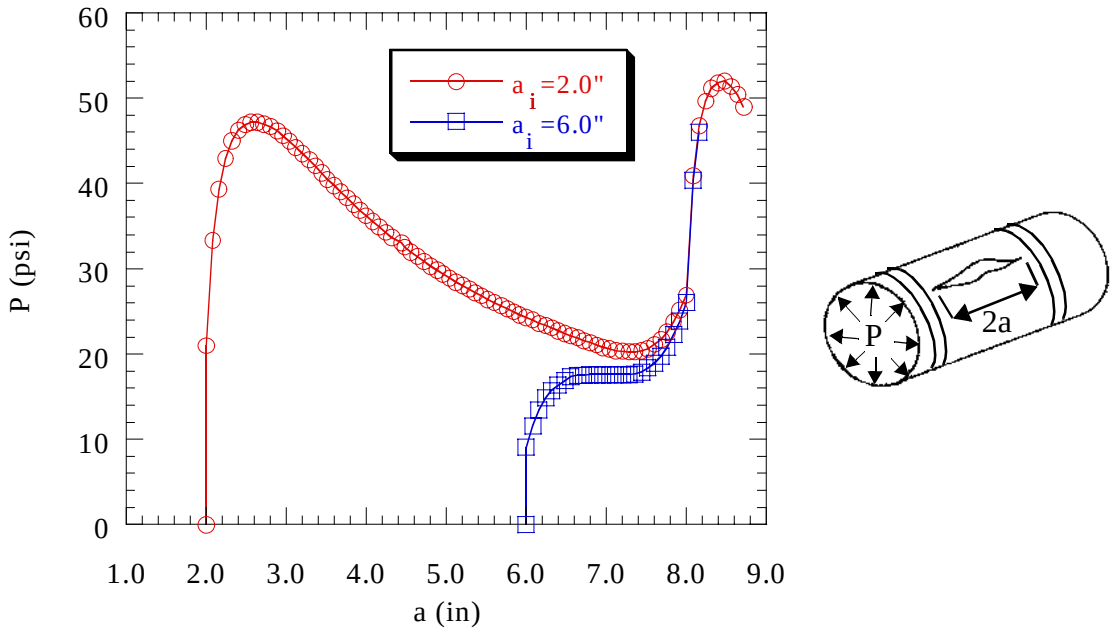

Fig. 5.2 Comparison of different initial half crack lengths on the crack growth curve.

5.3 Crack Turning Model Results

All five crack turning models contain approximately 5500 nodes, 31,000 degrees of freedom, and use the same solution file as previously described for correlating the model to the experiment. These models require the use of the solution file that does not involve the unstable crack growth algorithm because this algorithm can not manage multiple crack tips. Reference Appendix A for an example of this solution file.

5.3.1 Prediction of Crack Bifurcation Using CTOA

The resulting crack growth curves for all five crack turning models, as well as the crack growth curve for self similar crack growth, are shown in Fig. 5.3. An expanded view of

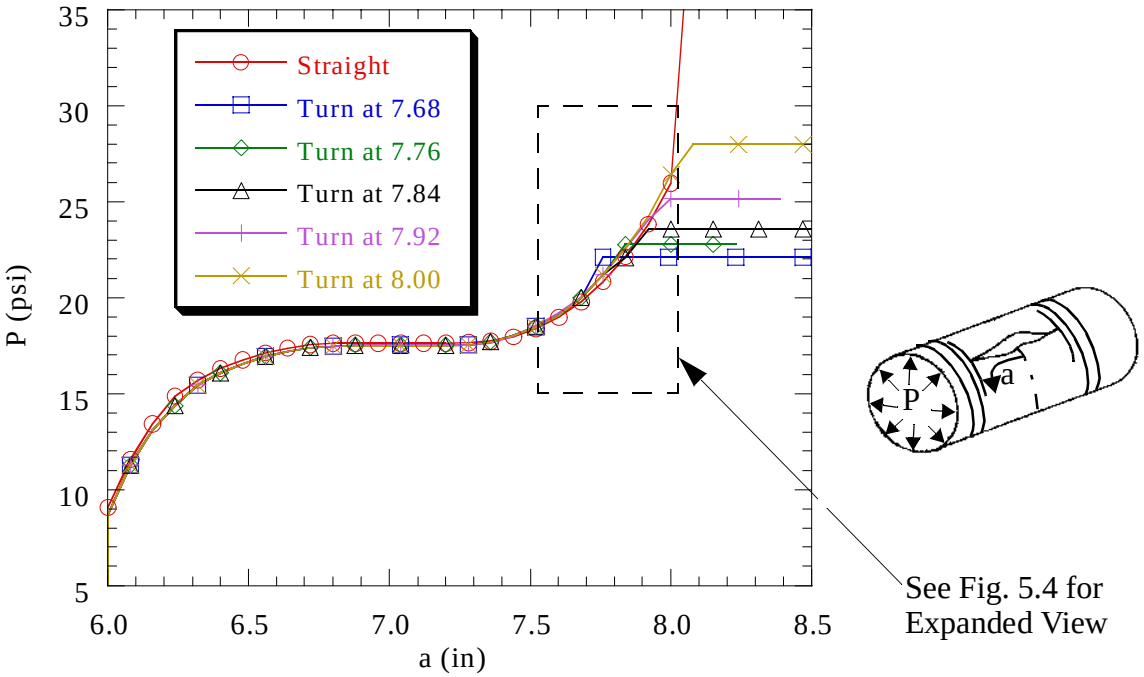

Fig. 5.3 Comparison of different crack turning paths.

the crack paths near the location of bifurcation in Fig. 5.3 is shown in Fig. 5.4. For half

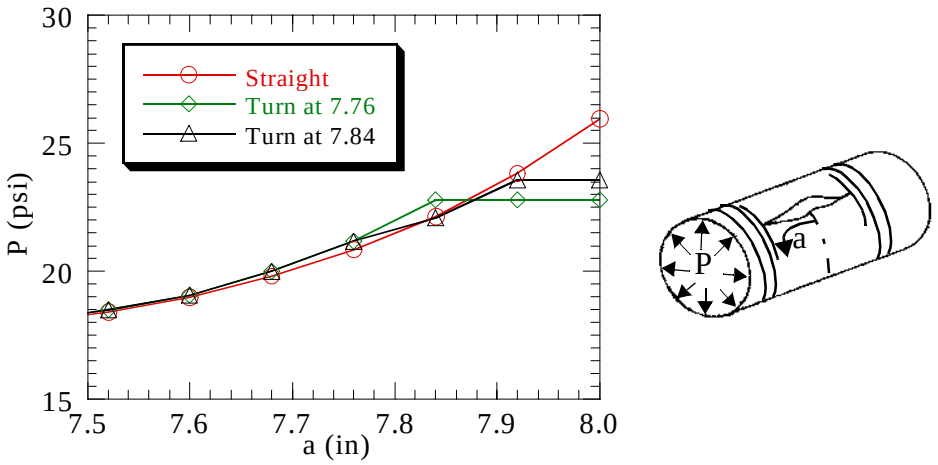

Fig. 5.4 Expanded view of the crack paths near the location of bifurcation.

crack lengths less than 7.60 inches, the crack growth curves are nearly identical to each other. However, as the five turning models force the crack into the circumferential direc-

tion, the curves from the crack turning models deviate from the self similar crack growth curve. In fact, once the crack turns into the circumferential direction the crack growth immediately becomes unstable for all five crack bifurcation locations. It can be seen in Fig. 5.3 and Fig. 5.4 that when the crack bifurcates at 7.68 inches and 7.76 inches the pressure required to open the first closed node in the circumferential direction is greater than the pressure to continue self similar crack growth. The other three locations of crack bifurcation all require less pressure to advance the crack in the circumferential direction than to proceed with self similar crack growth.

Assuming that the crack will grow along a path which provides the least resistance, the crack would not turn at the half crack length of 7.68 inches nor would it turn at 7.76 inches, since it would take a higher pressure to advance the crack in the circumferential direction than it would in the axial direction. However, since the pressure to bifurcate the crack at 7.84 inches (Fig. 5.4) is less than the pressure to continue self similar crack growth, the crack would be predicted to bifurcate before reaching a half crack length of 7.84 inches. Since the mesh dictates bifurcation locations separated by 0.080 inches, it is inferred that the crack will bifurcate at some point between half crack lengths of 7.76 and 7.84 inches. Hence, the analysis bounds the bifurcation point between 7.76 inches and 7.84 inches, which corresponds to the experimental result of the crack bifurcating at 7.77 inches.

5.3.2 Comparison With Published Crack Turning Criteria

Three stress based crack turning criteria are used to corroborate the STAGS crack turning results. To reiterate from Chapter 1, the first criterion is from Kosai and Kobayashi[12] and they infer crack turning when the ratio of axial stress to circumferential stress is greater than one. The second criterion is the maximum principal stress criterion[14], which postulates that crack growth will occur in a direction perpendicular to the direction of maximum principal stress. Finally, the maximum hoop stress criterion[14,15] is based on the notion that the crack will propagate in the direction perpendicular to the maximum hoop stress. This criterion was initially postulated for cracked flat plates, and the hoop stress is the normal stress component acting on the face normal to the polar angle defined in cylindrical coor-

dinates whose origin is at the crack tip. In application to cylindrical shells, it is confusing to call this the maximum hoop stress criterion since the hoop stress is the circumferential normal stress. We will call this criterion the maximum polar normal stress criterion. The polar normal stress is the stress component perpendicular to the face defined by a constant value of the angle between the axial direction and the helix emanating from the crack tip. See Fig. 5.5.

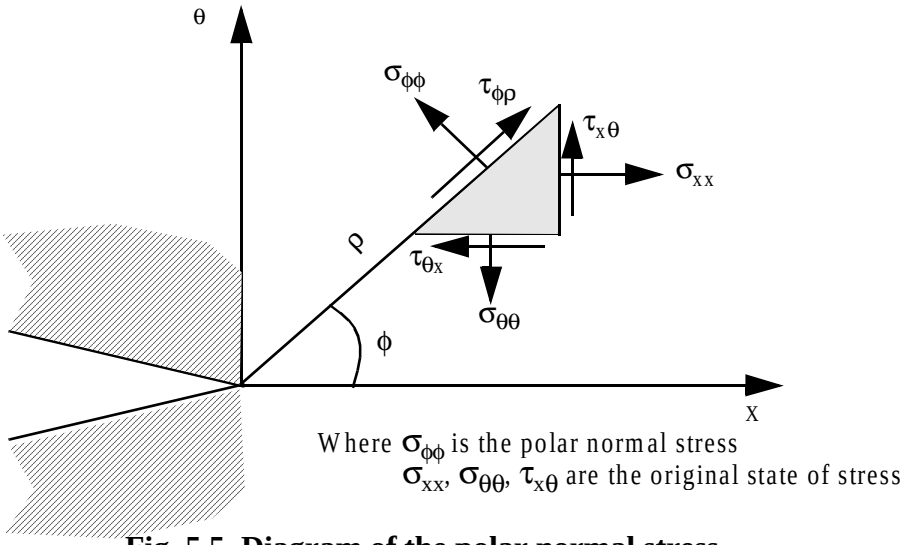

Fig. 5.5 Diagram of the polar normal stress.

This part of the study investigates the three criteria for the stress field ahead of the crack tip. The stress data used in the different crack turning criteria are taken from the results of the self similar crack growth model which was described in the previous chapter. Using this model also provides a second comparison of the results from a model with a six inch initial half crack length to a model with a two inch initial half crack length. To use the stress based criterion, the crack is grown from a half length of two inches to six different final half crack lengths of a = 3.04, 5.04, 7.04, 7.68, and 7.76 inches. The first three final half crack lengths correspond to cracks which are predicted in the analysis to remain self similar. The half crack length a = 7.68 inches corresponds to the threshold of the crack turning as predicted by the analysis, and a = 7.76 inches closely corresponds to the point of crack turning.

The first crack turning criterion applied to the STAGS self similar crack growth results considers the ratio of the axial stress to the circumferential stress at the centroid of the ele-

ments along the crack path and ahead of the crack tip. The stress ratio on the inner and outer surface of the cylinder for the five half crack lengths is shown in Fig. 5.6a and Fig. 5.6b.

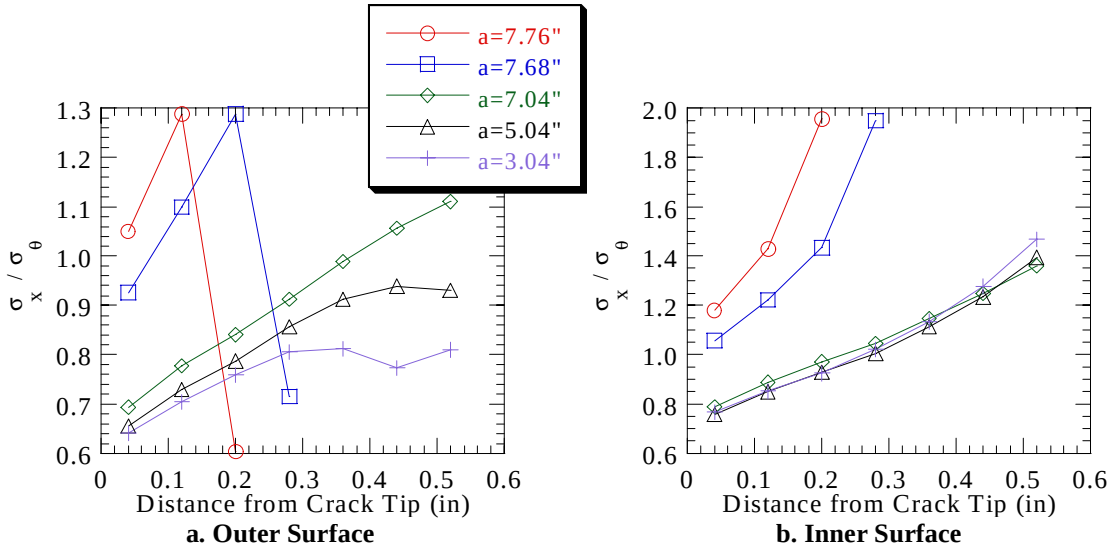

Fig. 5.6 Ratio of axial stress to circumferential stress for a 0.156 in. by 2.00 in. tear strap.

For the three smallest half crack lengths, both the outer and inner surface show the stress ratio of the element closest to the crack tip is always less than one. As the distance ahead of the crack tip increases, the stress ratio generally increases. Since the stress ratio ahead of the crack tip is less than one, the crack is predicted to propagate in a self similar manner. When the half crack length increases to 7.68 inches, the inner surface stress ratio for the elements ahead of the crack tip is greater than one, while the stress ratio on the outer surface is less than one. Once the half crack length increases to 7.76 inches, both stress ratios are greater than one for the two elements immediately ahead of the crack tip. This suggests crack turning when the half crack length is approximately 7.76 inches, which matches the predictions based on the $CTOA_c$ as well as the experimental results.

The maximum principal stress criterion also applies to the stresses immediately ahead of the crack tip. Again, only the first seven elements ahead of the crack tip are considered. The principal stresses are computed at the centroid of the elements both at the top and bot-

tom of the shell wall. The directions perpendicular to the maximum principal stress at the inner and outer surfaces of the cylinder are shown in Fig. 5.7a and Fig. 5.7b, respectively.

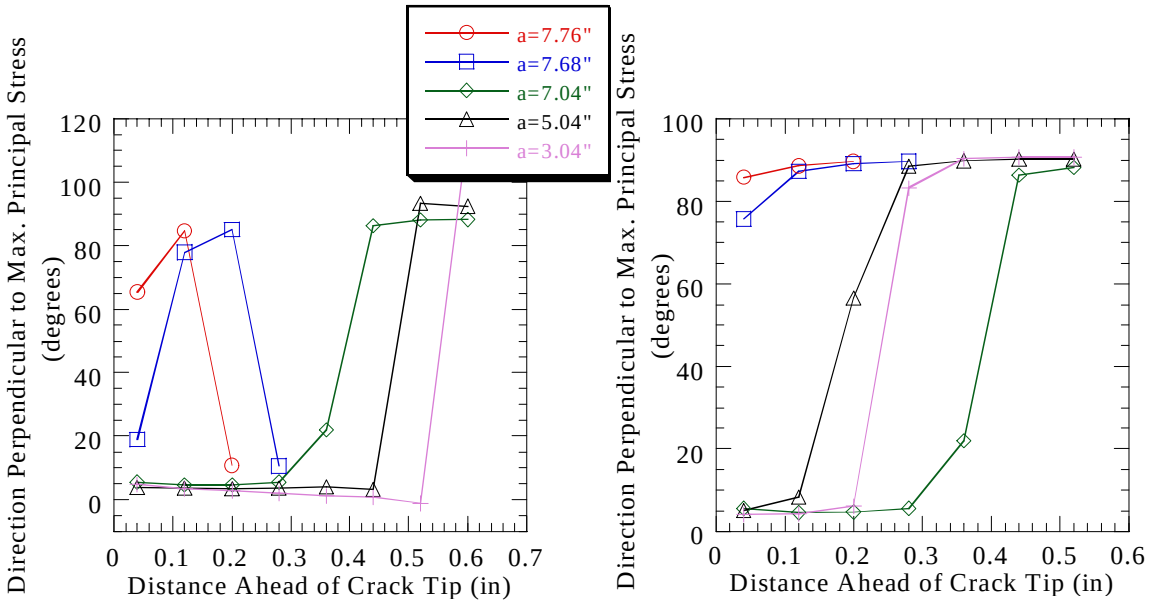

a. Outer Surface

b. Inner Surface

Fig. 5.7 Results of maximum principle stress criterion for a 0.156 in. by 2.00 in. tear strap.

The crack growth directions for both the inner and outer surfaces for half crack lengths of 3.04, 5.04, and 7.04 inches are well below 45°, which indicates that crack growth will continue in the axial direction. These results are expected since the crack did not turn for any of these half crack lengths. For the half crack length of 7.68 inches, just before the crack bifurcates, the normal to the maximum principal stress on the inner surface is much greater than 45° and approaches the circumferential direction (90°). However, the angle of propagation on the outer surface is much smaller than 45°. For the half crack length of 7.76 inches, just after the crack bifurcates, the direction perpendicular to the maximum principal stress on both the inner and outer surface is much greater than 45°. Hence, crack bifurcation is predicted and the maximum principal stress criterion corroborates the experimental and analytical results.

Applying the maximum polar normal stress criterion is slightly different than the other two criteria. This criterion incorporates not only the stresses along the crack path ahead of the crack, but the stresses above and ahead of the crack tip as well. Only the six elements

closest to the crack tip are considered for the five half crack lengths and the polar normal stress is calculated at the centroid of each element. The results for the five half crack lengths are shown in Fig. 5.8 through Fig. 5.12.

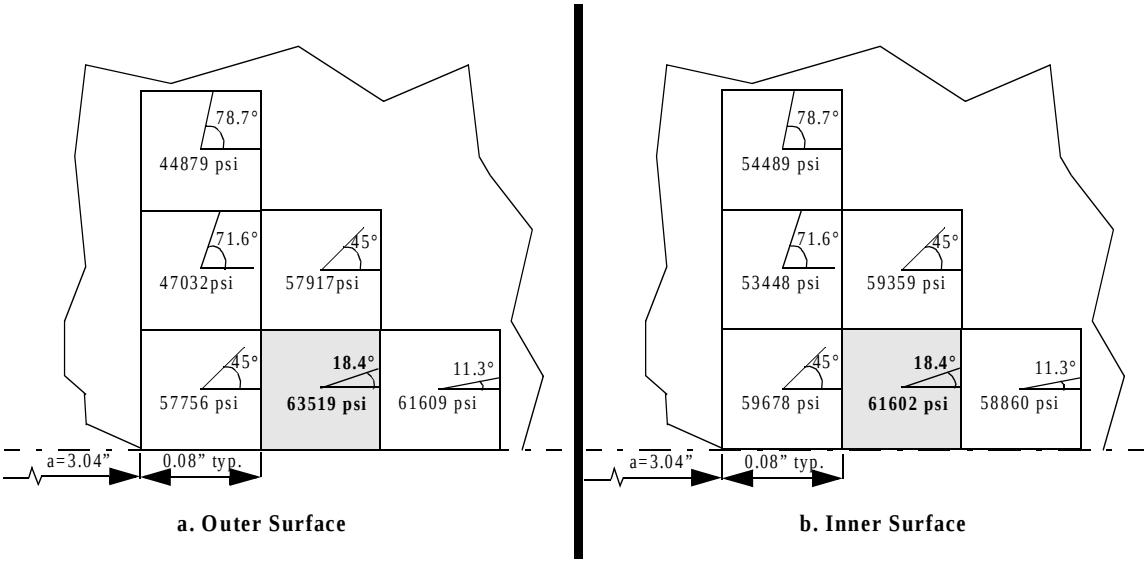

Fig. 5.8 Results of the maximum polar normal stress criterion for a=3.04 in.

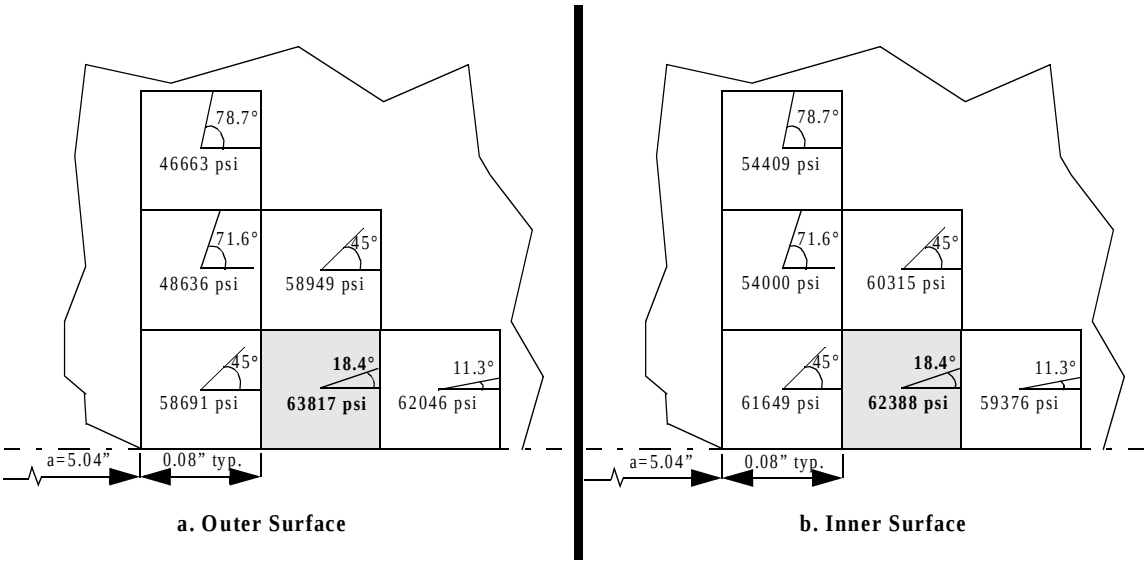

Fig. 5.9 Results of the maximum polar normal stress criterion for a=5.04 in.

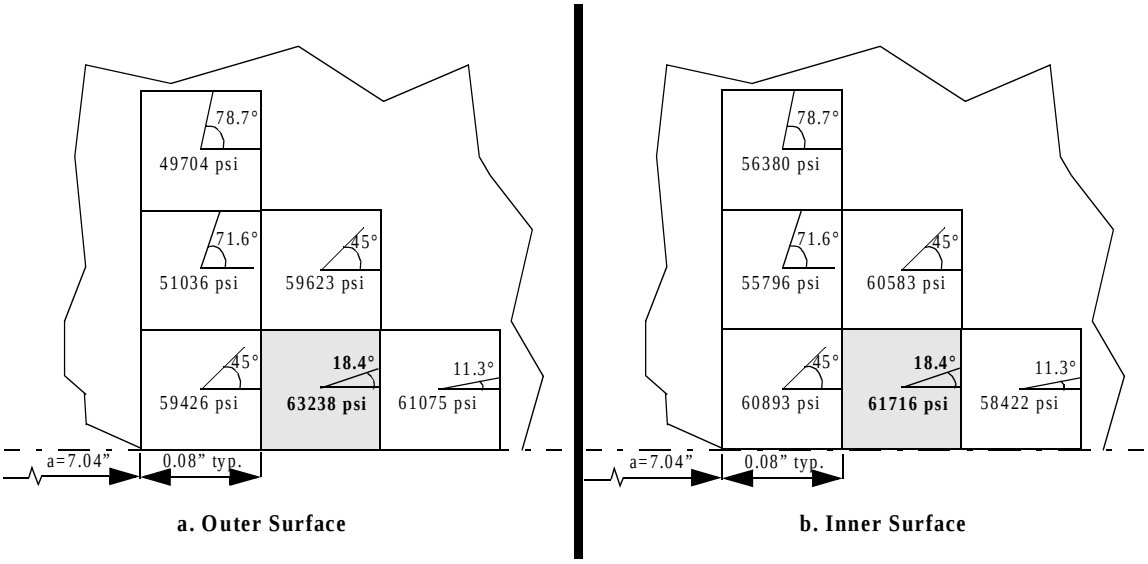

Fig. 5.10 Results of the maximum polar normal stress criterion for a=7.04 in.

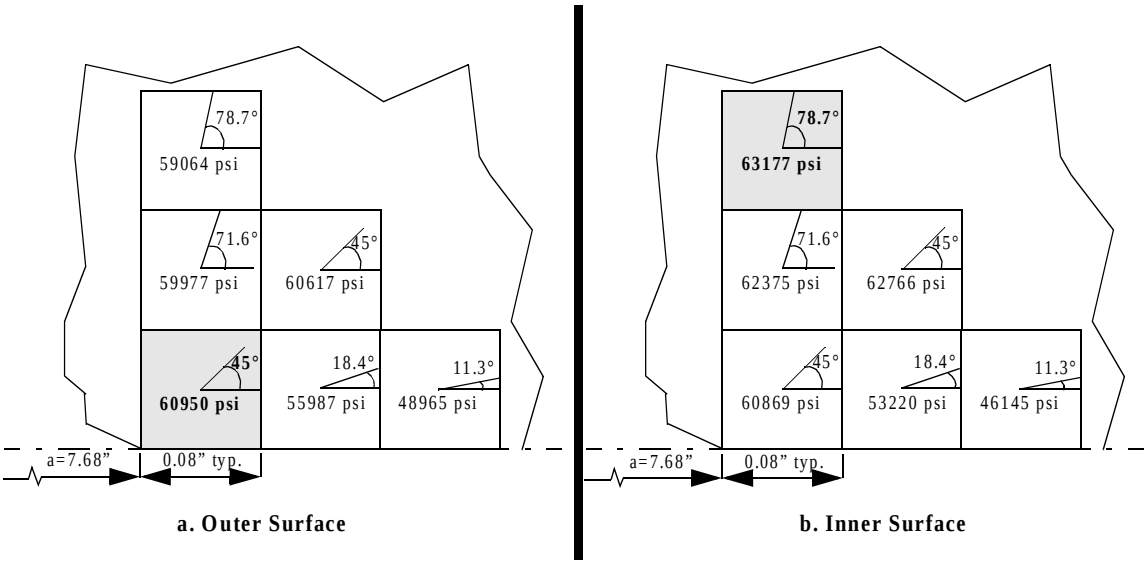

Fig. 5.11 Results of the maximum polar normal stress criterion for a=7.68 in., before the point of crack bifurcation.

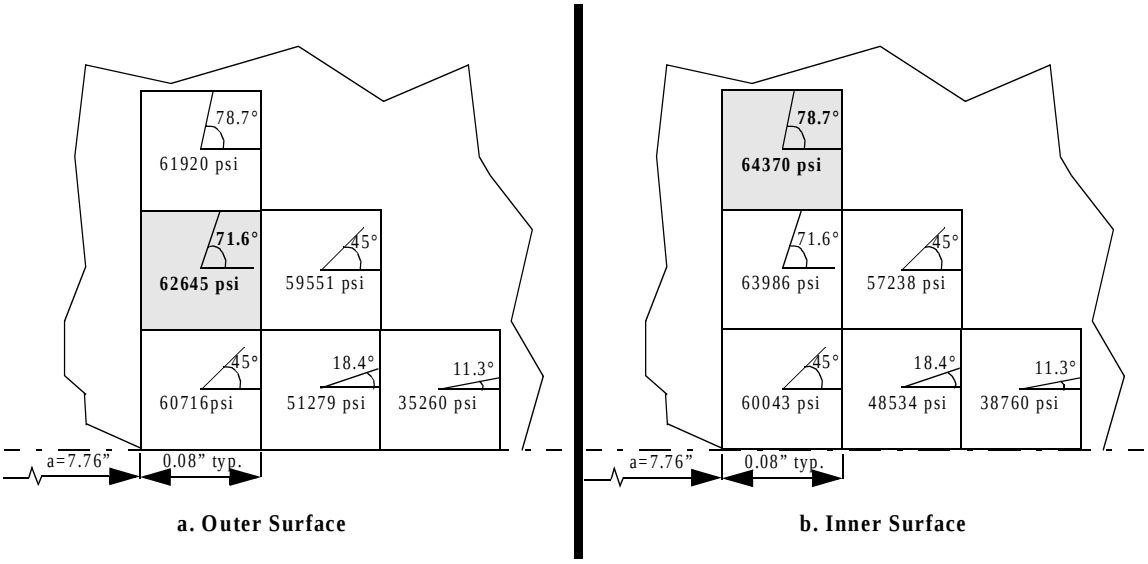

Fig. 5.12 Results of the maximum polar normal stress criterion for a=7.76 in., at the point of crack bifurcation.

The results of the maximum polar normal stress criterion are similar to the results from the two previously discussed criteria. For all three of the smallest half crack lengths, the maximum polar normal stress is in the element along the crack path two elements away from the crack tip. Since the direction normal to the maximum polar normal stress in Fig. 5.8, Fig. 5.9, and Fig. 5.10 are less than 45°, crack propagation in the axial direction is indicated. When the crack tip reaches the half crack length at the threshold of crack turning, the maximum polar normal stress on the inner surface shifts to the third element above the crack tip which indicates crack turning, see Fig. 5.11. At this crack length it is inconclusive if the crack will turn according to the stresses on the outer surface. This is because the maximum polar normal stress on the outer surface indicates crack growth at 45°. Once the half crack length reaches the STAGS predicted location of crack turning, Fig. 5.12, both the inner and outer surface results indicate crack turning.

5.4 Parametric Study of Various Tear Strap Sizes

Since the STAGS crack turning models and published crack turning criteria appear to accurately predict the location of crack bifurcation, these methods are used to assess the ability of tear straps of various sizes to induce flapping. The parametric quantities associ-

ated with the tear straps include the thickness, width, spacing, and material properties. Using all four variables in a parametric study would take large amounts of time and computer resources. To maintain a reasonably sized study, only the thickness and width of the tear straps are varied.

5.4.1 Unstiffened Cylinder

The first case of a parametric study on strap thickness to be considered here is that of a cylinder that does not contain a tear strap. The purpose of this case is to verify if flapping can occur without tear straps in a 16-inch long cylinder. Flapping in unstiffened cylinders has been demonstrated experimentally by Swift.[2] The resulting crack growth curves from the self similar crack growth model of the unstiffened cylinder to the results of the cylinder stiffened by the experimental tear strap are shown in Fig. 5.13. For the unstiffened shell, the pressure continues to decrease as the half crack length exceeds 8.0 inches. The results shown in Fig. 5.14 indicate that the crack will not turn at half crack lengths less than 8.0 inches without the presence of a tear strap. Since it requires more pressure to turn

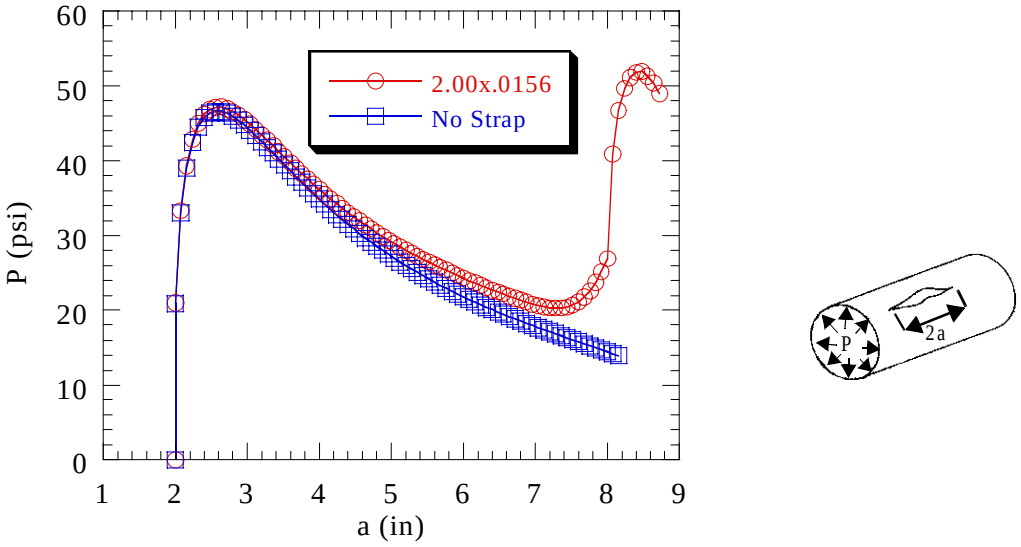

Fig. 5.13 Effect of the tear straps on self similar crack growth.

the crack at the five turning locations, the crack will continue to follow the self similar path.

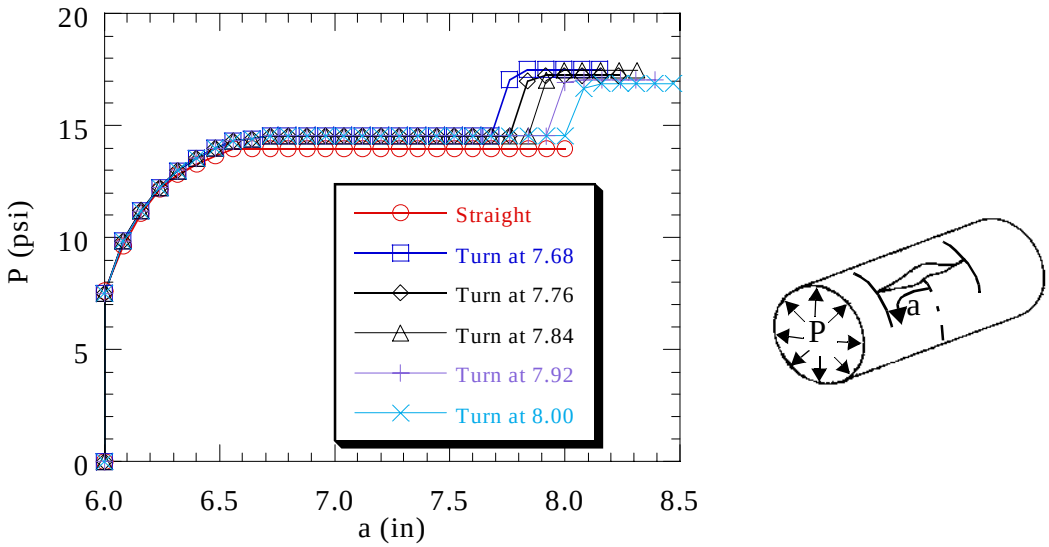

Fig. 5.14 Comparison of different crack paths in an unstiffened cylinder.

5.4.2 Effect of Tear Strap Thickness on the Behavior of a Crack

Evaluating the effect of tear strap thickness on the behavior of a crack involves analyzing thicknesses both larger and smaller than the thickness used in the experiment. The tear strap thicknesses analyzed in STAGS are selected from commonly available stock sizes of 2024-T3 aluminum.

Based on 2024-T3 aluminum stock sizes, tear strap thicknesses of 0.190 inch, 0.08 inch, 0.04 inch, and 0.02 inch are chosen for analysis. In order to investigate only the effect of thickness, the width of the tear strap remains identical to the experimental tear strap, which is 2.0 inches wide. All four thicknesses are analyzed in the self similar crack growth model as well as the five crack turning models. The input files and solution files are identical to the files described in Section 4.2 and Section 5.2 with the obvious exception of a few modifications to account for the tear strap thicknesses.

5.4.2.1 Results of Self Similar Crack Growth

The effect of tear strap thickness on the crack growth curve as produced by the self similar crack growth model is shown in Fig. 5.15. It is clear from the figure that the tear

strap thickness has a considerable effect on the behavior of the crack both before and after the crack defeats the tear strap. In the region of stable crack growth, the crack growth curve is essentially independent of the tear strap thickness. For half crack lengths less than 5.0 inches, the crack growth curves are nearly the same. However, once the crack exceeds a half crack length of 5.0 inches, the thicker tear straps require a greater pressure to further advance the crack. Also, the location of minimum pressure moves away from the edge of the tear strap as the thickness increases. Once the crack defeats the tear strap, the maximum pressure attained within the tear strap increases as thickness increases. Also note for the thickness of 0.02 inch, the crack growth inside the tear strap attains its maximum pressure almost immediately, or within 0.08 inches of crack growth inside the strap.

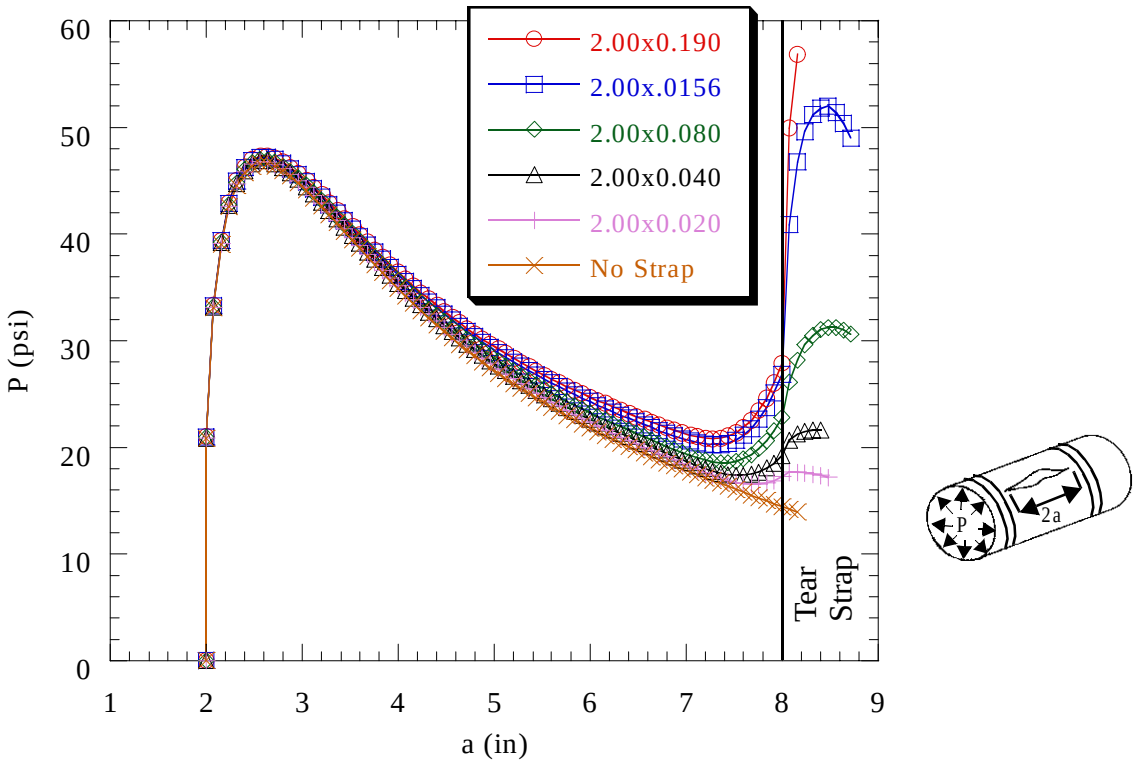

Fig. 5.15 Effect of tear strap thickness for self similar crack growth.

5.4.2.2 Results of Crack Turning Models

The four variations of tear strap thickness are accommodated in the five crack turning models and in the self similar crack growth model with the initial half crack length of six

inches. The crack turning results for the tear strap thicknesses of 0.190 inch, 0.080 inch, 0.040 inch, and 0.020 inch are shown in Fig. 5.16 though Fig. 5.19, respectively.

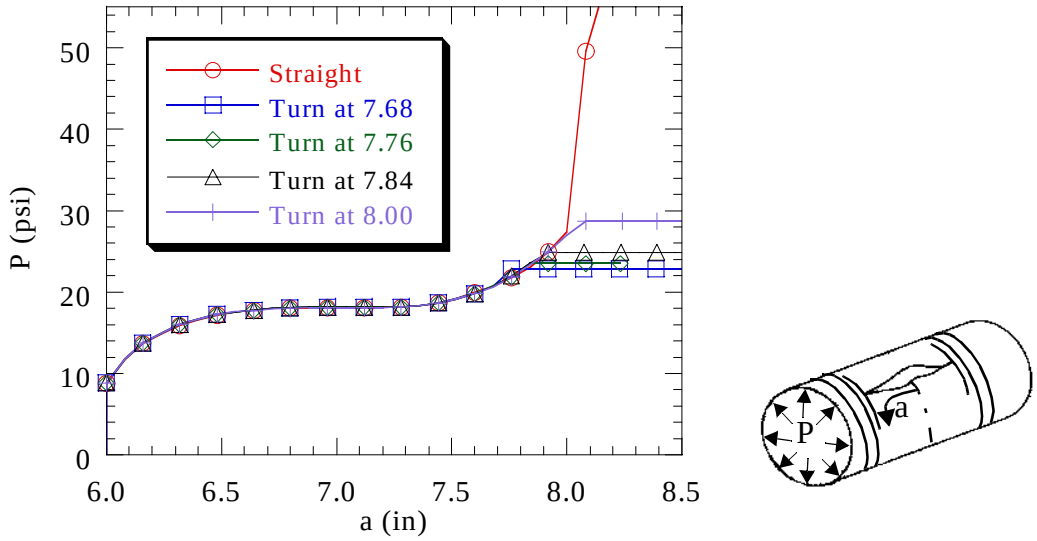

Fig. 5.16 Comparison of different crack paths for a 0.190 in. thick tear strap.

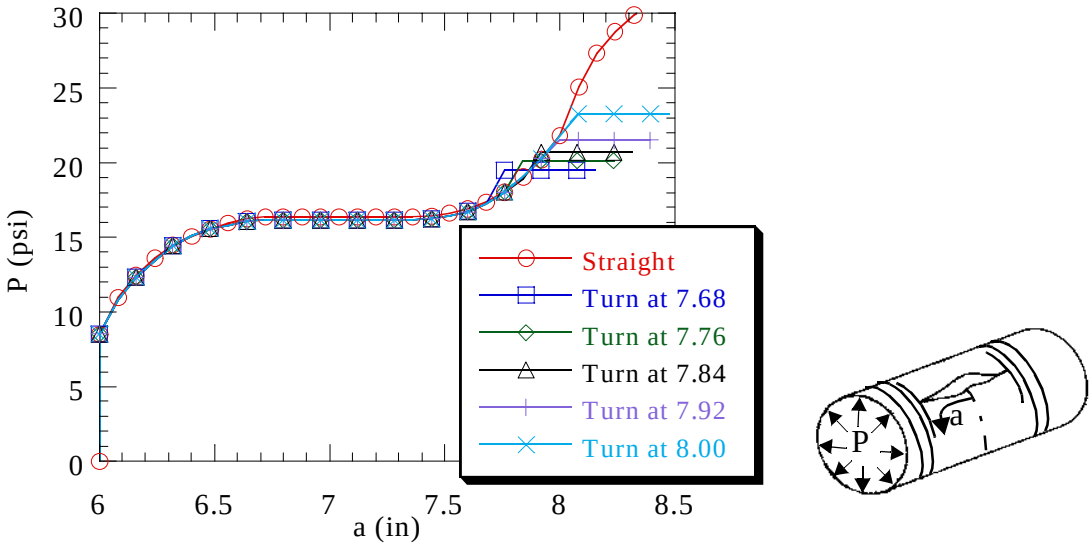

Fig. 5.17 Comparison of different crack paths for a 0.08 in thick tear strap.

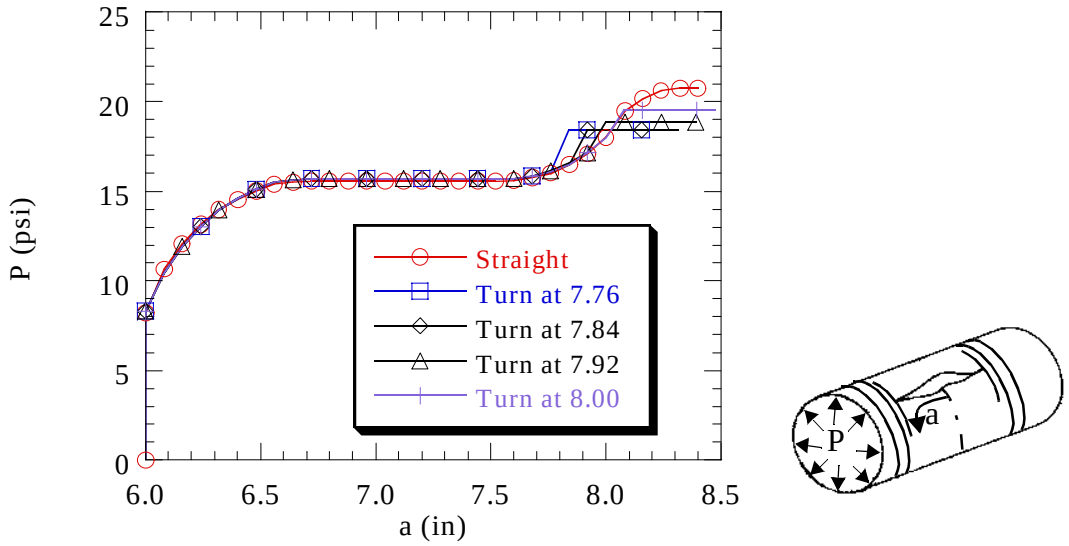

Fig. 5.18 Comparison of different crack paths with a 0.04 in. thick tear strap.

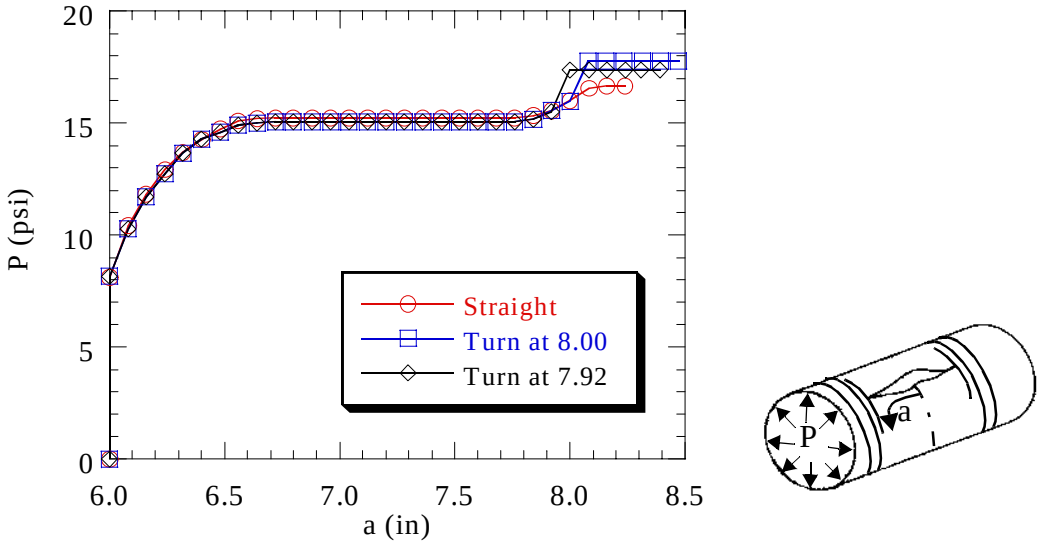

Fig. 5.19 Comparison of different crack paths with a 0.02 in. thick tear strap.

As shown in Fig. 5.16, it takes more pressure to open the first node in the circumferential direction if the crack turns at half crack lengths of 7.68 inches than to continue self similar crack growth. However, it takes less pressure to propagate a crack along bifurcated paths at 7.76 inches, 7.84 inches, or 8.00 inches, than it does for self similar growth. Applying the same logic used for the interpretation of the results generated from the

experimental specimen, crack turning in a cylinder stiffened by a 0.190 inch by 2.00 inches tear strap should occur between the half crack lengths of 7.68 inches and 7.76 inches.

In the same manner, the crack growth curves for the thicknesses of 0.08 inches (Fig. 5.17) and 0.04 inches (Fig. 5.18), seem to indicate that decreasing the tear strap thickness decreases the distance between the location of crack turning and the edge of the tear strap. For the 0.08 inch thick tear strap, the results appear to indicate crack turning between half crack lengths of 7.84 inches and 7.92 inches. In the case of a 0.04 inch thick tear strap, the location of crack turning is between half crack lengths of 7.92 inches and 8.00 inches. This trend is expected since reducing the thickness of the tear straps reduces the ability of the strap to toughen the cylinder, thus inducing flapping at longer half crack lengths.

The tear strap thickness of 0.02 inches provides results different than previously discussed. Only two crack turning locations are considered for this thickness, based on the assumption that the trend of the turning location will continue to shift toward the edge of the tear strap. Since the results of the tear strap thickness of 0.04 inches suggest turning will occur after a half length of 7.92 inches, only the models which turn the crack at half crack lengths of 7.92 and 8.00 are used. These results, shown in Fig. 5.19, indicate that less pressure is needed to continue self similar crack growth than needed for turning the crack at either half crack lengths. Therefore, it is predicted that the 0.02 inch thick tear strap is not capable of inducing flapping. Rather, the crack will defeat the tear strap.

5.4.2.3 Comparison With Published Crack Turning Criteria

The comparison with the published crack turing criteria, mentioned in Section 5.3.2, is limited to only the tear strap with a thickness of 0.04 and 0.02 inches. These two sizes are chosen since the 0.04 inch thick strap represents the thinnest tear strap in which STAGS analysis predicts crack bifurcation between half crack lengths of 7.92 and 8.00 inches, and the 0.02 inch tear strap size which did not indicate crack turning. A comparison with the results of the published crack turning criteria becomes necessary in order to establish confidence in the STAGS results.

All three previously discussed crack turning criteria are applied to the two chosen tear strap thicknesses. Again the stress data for applying the different crack turning criteria is taken from the results of the self similar crack growth model. For the application of the stress based crack turning criteria, four half crack lengths are chosen to look at the behavior of the stresses near the crack tip. The crack is grown from an initial half length of two inches to final half crack lengths of 7.04 inches, 7.76 inches, 7.84 inches, and 7.92 inches. These criteria are only applied in the region between the crack tip and the tear strap edge.

The ratio of axial to circumferential stresses at the centroid of the elements ahead of the crack tip is shown in Fig. 5.20a and b at the outer and inner surfaces of the shell with a 0.04 inch thick tear strap. The crack growth directions for both the outer and inner sur-

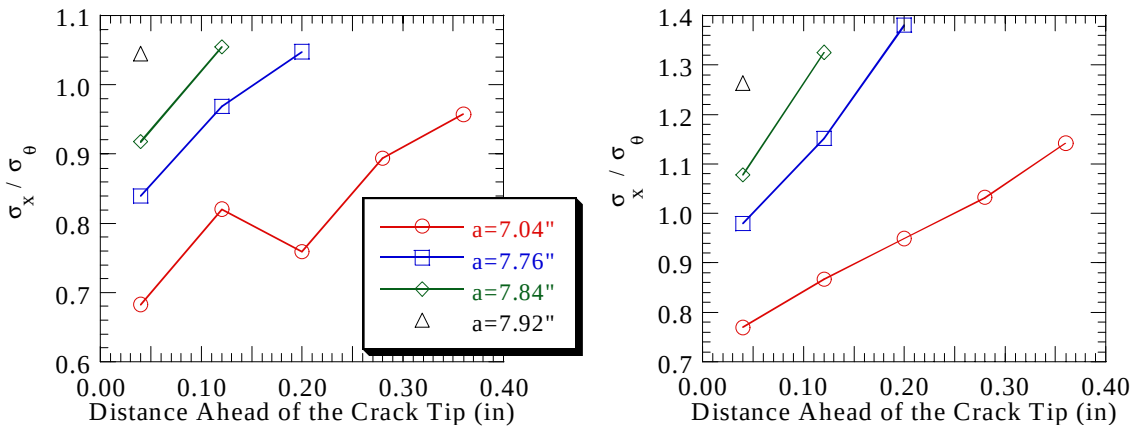

a. Outer Surface **b. Inner Surface**

Fig. 5.20 Stress ratio results for a 0.04 in. by 2.00 in. tear strap.

faces for half crack lengths of 7.04 and 7.76 inches do not indicate crack growth in the circumferential direction. For the half crack length just before the STAGS predicted location of crack turning, the stress ratio on the inner surface is greater than unity, indicating crack turning, while the outer surface ratio is less than one. This does not indicate crack turning as the ratio is less than one. However, the stress ratio on the inner and outer surfaces becomes greater than one for the half crack length of 7.92 inches, indicating crack turning. These results correlate with the STAGS predicted results.

Results for the stress ratio on the outer and inner surface of the 0.02 inch thick tear strap are shown in Fig. 5.21a and b These results also corroborate the results predicted using the CTOA criterion. For each of the half crack lengths, the stress ratio for the element closest to the crack tip is less than one. This indicates that the crack growth direction will remain in the axial direction and the crack will not turn before reaching the tear strap.

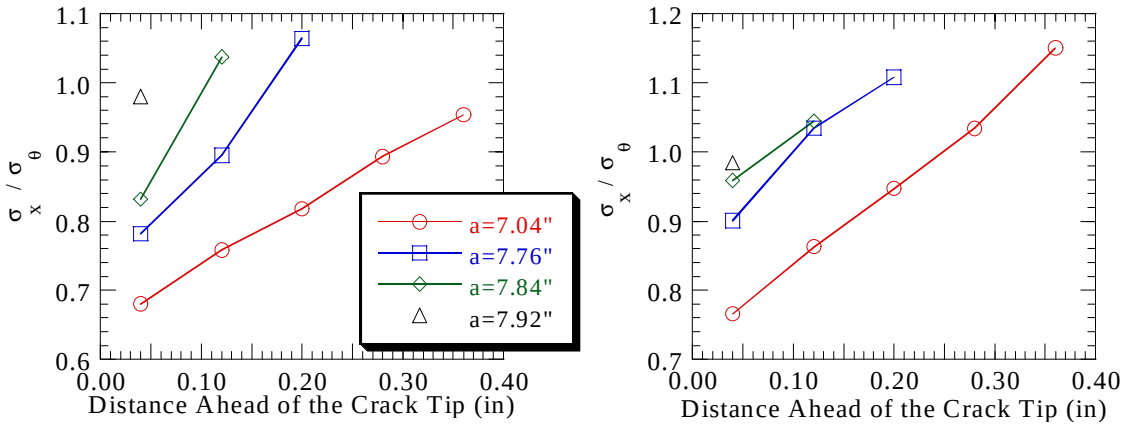

a. Outer Surface **b. Inner Surface**

Fig. 5.21 Stress ratio results for a 0.02 in. by 2.00 in. tear strap.

The maximum principal stresses are calculated at the centroid of the element for the elements ahead of the crack tip. Results of the determination of the direction perpendicular to the maximum principal stress are shown in Fig. 5.22a and b.and Fig. 5.23a and b for the outer and inner surfaces for the analytical models with a 0.04 and 0.02 inch tear strap, respectively. These results are similar to those found from studying the stress ratios. Again the half crack lengths of 7.04 and 7.76 inches indicate the crack growth direction is more aligned with the axial direction for both tear strap thicknesses. The 0.04 inch thick tear strap suggests crack turning at a half crack length of 7.92 inches as the direction of crack growth for both the inner and outer surface, is more aligned with the circumferential direction.For the 0.02 inch thick tear strap, the crack growth direction is predicted to be in the

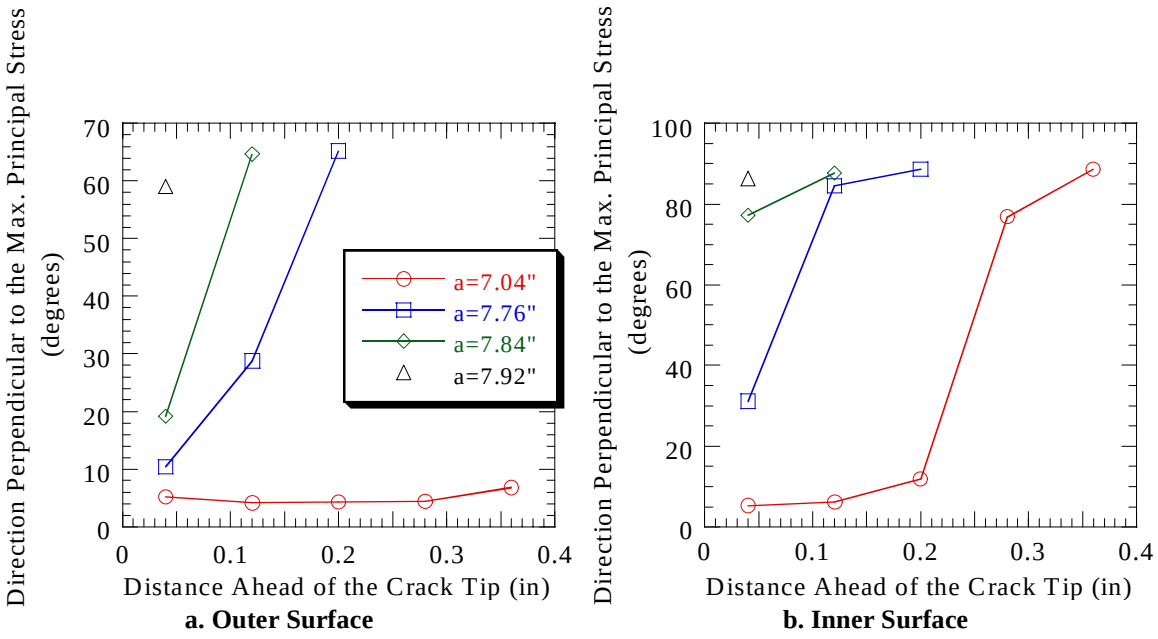

Fig. 5.22 Maximum principal stress criterion at various half crack lengths for a 0.04 in. by 2.0 in. tear strap.

axial direction for all half crack lengths, suggesting the crack will not turn. The results for both thicknesses agree with the results predicted by the STAGS analysis.

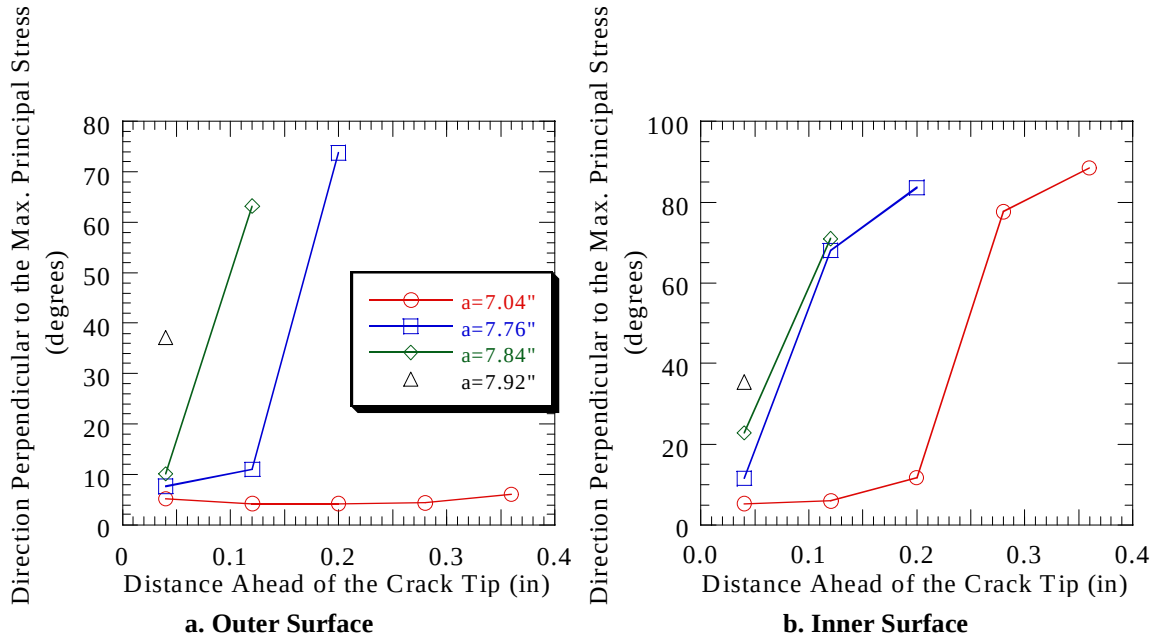

Fig. 5.23 Maximum principal stress criterion at various half crack lengths for a 0.02 in. by 2.0 in. tear strap.

Finally, the maximum polar normal stress is calculated at the centroid of the elements surrounding the crack tip. For brevity, only the results of the maximum polar normal stress criterion applied at the half crack length of 7.92 inches are presented here for both tear strap thicknesses, and are shown by Fig. 5.24 and Fig. 5.25. The results for the three remaining half crack lengths can be seen in Appendix B, where is it shown that all cases indicate either axial crack growth or inconclusive results. As shown in the Fig. 5.24, crack

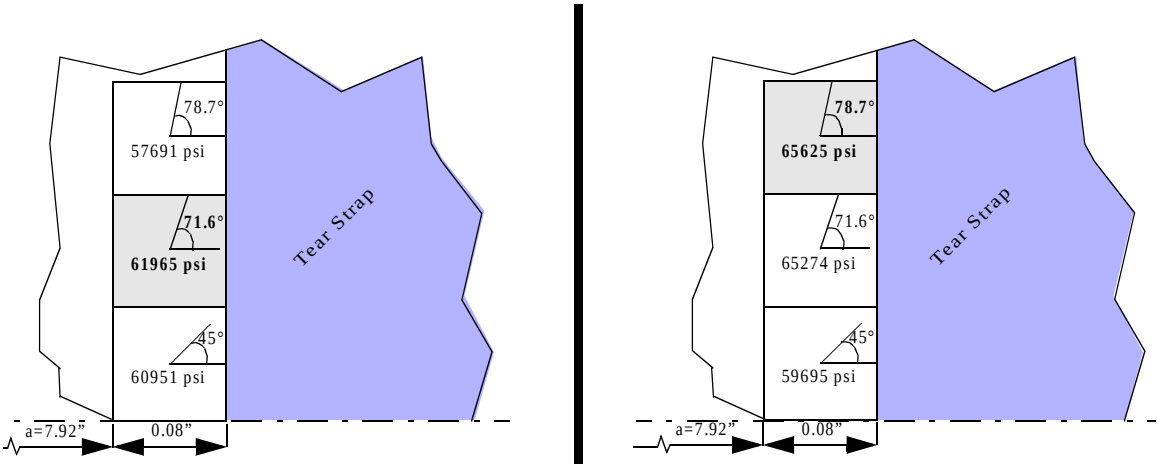

Fig. 5.24 Maximum polar normal stress criterion for a 0.04 in. by 2.00 in. tear strap.

turning into the circumferential direction is predicted to occur at a half crack length of 7.92 inches for the 0.04 inch tear strap. This result agrees with the STAGS prediction. Fig. 5.25 shows the results for the 0.02 inch tear strap. Unfortunately, the results for the 0.02

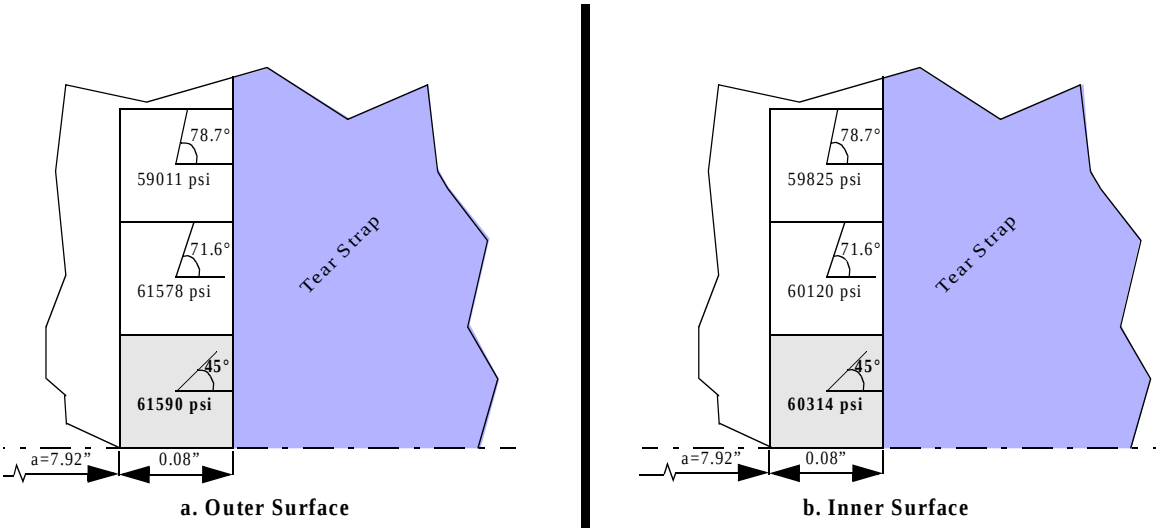

Fig. 5.25 Maximum polar normal stress criterion for a 0.02 in. by 2.00 in. tear strap.

inch thick tear strap are inconclusive. This is because the polar normal stress on the inner and outer surface predicts a crack growth angle of 45°, a value which is neither axial or circumferential.

5.4.3 Effect of Tear Strap Width on the Behavior of a Crack

The effect of tear strap width on crack bifurcation is investigated on a tear strap narrower than the one used in the experiment. In this portion of the parametric study, the width of the tear strap is selected for modeling convenience to be 0.96 inches. The thickness of the strap is 0.156 inches, the same as the experiment. As with the previous analyses, the narrower tear strap is analyzed using the self similar crack growth model and the five crack bifurcation models.

5.4.3.1 Results of Self Similar Crack Growth

The crack growth curves resulting from a self similar crack path encountering the 0.96-inch-wide and the 2.00-inch-wide tear straps are shown in Fig. 5.26. From this figure it is clear that the width of the tear strap affects minimally the behavior of the crack growth curve before the crack enters the tear strap. As observed with the effects of thick-

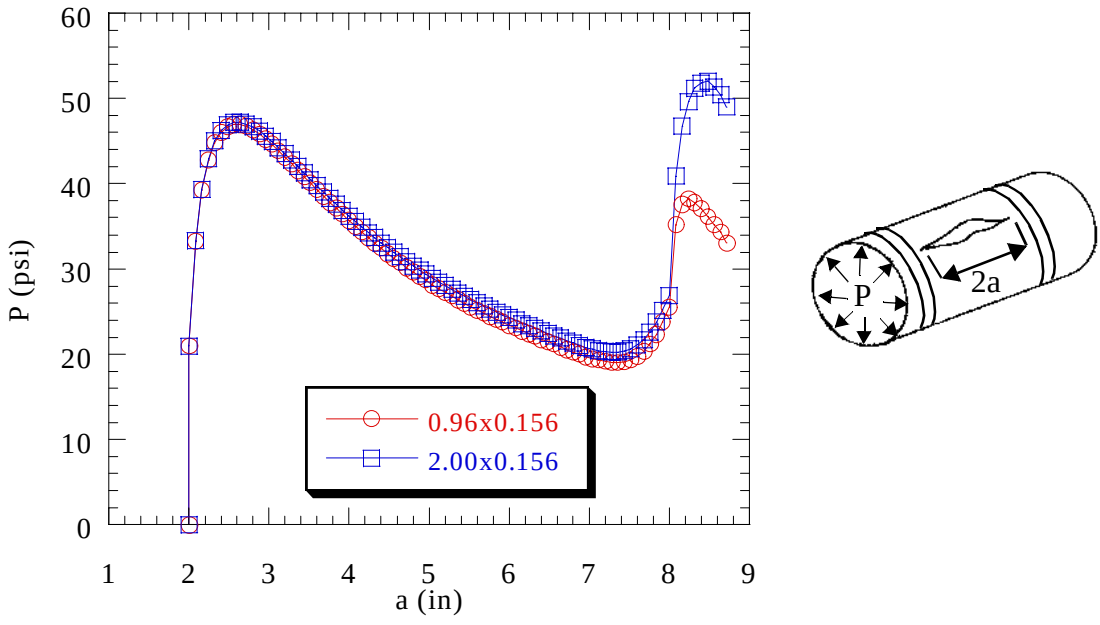

Fig. 5.26 Effect of tear strap width on self similar crack growth.

ness, the results of stable crack growth are independent of the width of the tear strap. Once unstable crack growth begins, the curves remain very similar. It does appear that the narrower the tear strap, the lower the minimum pressure. However, the location of the minimum pressure is about the same for both tear strap sizes. After the crack enters the tear strap, there is a large difference between the curves. The narrower tear strap not only reduces the maximum pressure inside the tear strap, but generates a maximum pressure at a shorter half crack length. Because this result is very similar to the results of the two inch wide tear strap, the effect of width on flapping is considered small and other widths are not considered.

5.4.3.2 Crack Turning Model Results

Since only one other tear strap width is considered by the current study, the crack turning models are only applied to a tear strap with cross-sectional dimensions of 0.156 inch by 0.96 inch. The results of the crack turning models and the self similar crack growth model, with an initial half crack length of six inches, are shown in Fig. 5.27. All of the crack growth curves behave in a similar manner as the results of the previous crack turning models. The results show that the crack path, which turns at a half crack length of 7.76 inches, requires a larger pressure than the self similar crack growth curve to advance the crack. See Fig. 5.28. When the crack turns at a half crack length of 7.84 inches, less pres-

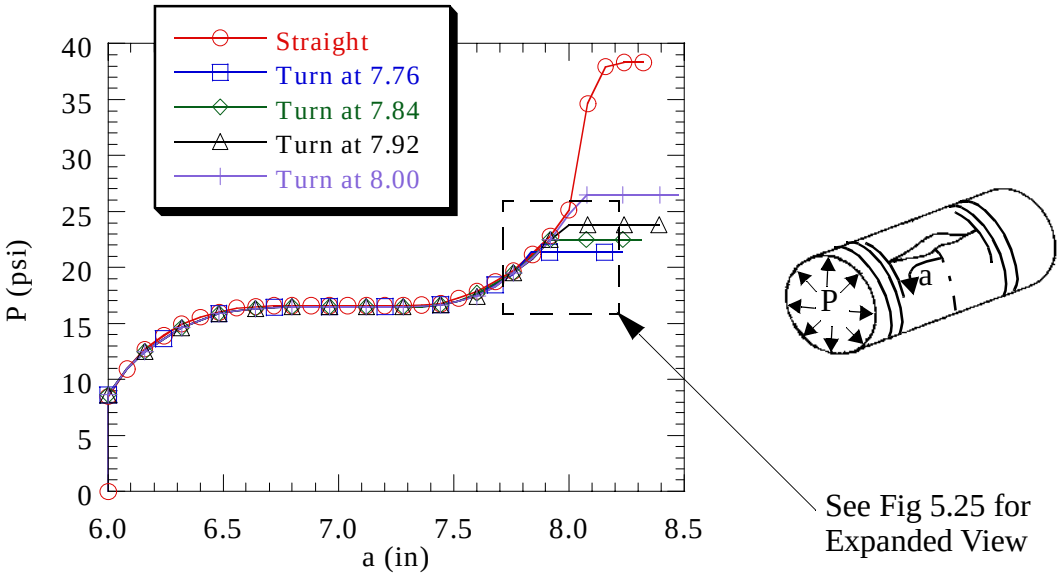

Fig. 5.27 Comparison of crack turning paths for a 0.156 in. thick by 0.96 in. wide tear strap.

sure is necessary to advance the crack in the circumferential direction than to continue the crack along the self similar crack path. Hence, the STAGS results bound the location of crack turning between half crack lengths of 7.76 inches and 7.84 inches.

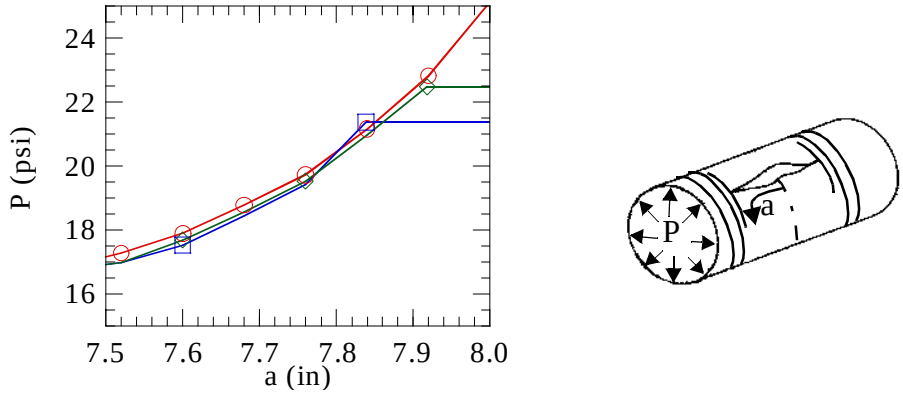

Fig. 5.28 Expanded view of region of where crack bifurcation is expected.

5.5 Discussion

STAGS analyses were conducted to predict the point of bifurcation for pressurized cylinders with various tear strap sizes. Experimental results were used to validate the STAGS model for one tear strap configuration. A summary of the tear straps analyzed in this study, the fast crack pressure in the tear strap, and the location of crack bifurcation is shown in Table 5.1. As shown in the table, changing the thickness has a larger effect on the location of bifurcation and the fast crack pressure.

Table 5.1 Summary of parametric study of various tear strap sizes.

Tear strap thickness (in)	Tear strap width (in)	A_{strap} (in^2)	Ratio[a] of EA_{strap} to EA_{total}	Fast crack pressure in tear strap (psi)[b]	Predicted location of turning (in)
0.190	2.00	0.380	0.345	>61.60	7.72 ± 0.04
0.156[c]	2.00[c]	0.312	0.302	52.21	7.80 ± 0.04
0.08	2.00	0.160	0.182	31.13	7.88 ± 0.04
0.04	2.00	0.080	0.100	20.77	7.96 ± 0.04
0.02	2.00	0.040	0.053	16.67	>8.00
0.156	0.96	0.150	0.172	38.37	7.80 ± 0.04

a. $A_{total} = A_{strap}$ + shell thickness times the distance between the centers of two tear straps
b. Pressure determined from an analysis with an initial half crack length of 6.0 inches. Note that for an initial half length of 2.0 inches, the fast crack pressure in the shell wall is 47.7 psi.
c. Indicates the size used in the experiment

Application of published crack turning criteria with the results of the STAGS self similar crack growth model also corroborated with the experimental results. The results of the crack turning criteria also show that the stresses on the inner and outer surface can be significantly different for various tear strap sizes. This is because in the vicinity of the tear strap, bending has a significant influence on the stress distribution through the thickness of the shell wall. As the crack tip approaches the tear strap the stress gradients may be severe enough to cause the crack to slant rather than to remain flat.

Continuation of this study requires experimental verification of the predicted crack turning results. Experimental results would provide valuable information for refining the analytical models. With improved analytical models, a more inclusive parametric study should be conducted which could include varying the material of the tear strap, the tear strap spacing, and even the cylinder radius.

There is also room for improvements to the analytical model. The assumption of an integral tear strap should be replaced with one in which the strap is bonded to the skin, so that a crack can propagate in the skin under the strap. The ability to model the adhesive layer has recently become available in STAGS with the introduction of the 840 sandwich

elements and the corresponding sandwich transition elements. Unfortunately, at this writing the sandwich transition elements are not fully functional and many difficulties were encountered in an attempt to add the adhesive layer. The inclusion of the adhesive layer is important since the adhesive layer will change how the stresses in the cylindrical shell are transferred to the tear strap. Other forms of shell/tear strap assembly could also be modeled, such as by the inclusion of rivets with or without an adhesive layer.

Another recommendation for improving the model is to incorporate into the analysis the dynamic effects of crack propagation. The inclusion of dynamic effects could add more accuracy to the predicted results. Unfortunately, the dynamic values of the allowables are extremely difficult to measure. Currently the STAGS code does not have this capability and the inclusion of a dynamic analysis could very easily exceed today's computational resources.

CHAPTER 6 Summary and Conclusions

6.1 Summary

The objective of this study is to investigate the mechanics of ductile fracture on the path of an initially axial crack approaching a tear strap in a pressurized aluminum cylindrical shell. An experiment of a circumferentially stiffened cylindrical shell, which provided the motivation for this study, was performed at the Structural Mechanics Branch of the NASA Langley Research Center. This experiment resulted in a fast crack pressure of 46.52 psi, 0.56 inches of stable crack growth, bifurcation of the crack path 0.23 inches before the tear strap, followed by crack growth in the circumferential direction, parallel to the edge of the tear straps.

An investigation into the mechanics of the fracture is performed through a numerical analysis for the static, nonlinear response of the test specimen using a ductile fracture criterion for the crack growth. The numerical analysis is conducted using version 3.0 of the STAGS[19] computer code. The ductile fracture criterion predicts crack growth if the crack tip opening angle (CTOA) is equal to, or exceeds, a critical value ($CTOA_c$). Experimental data for the fast crack pressure, amount of stable crack growth, and far field strains are used to establish a value for the $CTOA_c$ and validate the modeling. A parametric study is conducted to find a value of the $CTOA_c$ which yields a fast crack pressure and length of crack stable growth which correlates with experimental data. This parametric study results

in a $CTOA_c$ of 5.0°. For $CTOA_c$ = 5.0°, the analysis predicts a fast crack pressure only 2.5% greater than the experimental results and with 0.64 inches of stable crack growth. The analysis with this choice of the $CTOA_c$ also shows excellent agreement between the experimental and analytical far field strains. Therefore, a $CTOA_c$ of 5.0° is used throughout this study.

With confidence established in the analytical model, crack growth is allowed to continue beyond the region of stable crack growth. The self similar crack growth model is analyzed twice, once using the stable crack growth algorithm and a second time using both the unstable and stable crack growth algorithms. The crack growth curve resulting from only using the stable crack growth algorithm is similar to an experimentally determined crack growth curve in the sense that the pressure can not decrease after the fast crack pressure has been achieved. Since the unstable algorithm can decrease the pressure from the fast crack pressure as the crack length advances, the details of the unstable portion of the crack growth are observed. As the axial crack approaches the toughened structure at the tear strap, a relative minimum pressure occurs and an increase in pressure is required to further advance the crack. Once the crack penetrates the tear strap even more pressure is necessary to advance the crack. Comparing the resulting crack growth curves indicates that self similar crack growth completely through the tear strap is unlikely, since the relative maximum pressure in the strap exceeds the fast crack pressure.

Since a self similar crack path did not occur in the experiment, several STAGS models with bifurcated crack paths were created. The modified crack paths are symmetric about the axis of the self similar path, and the turning angle at the point of bifurcation is 90°. Five separate models are developed to turn the crack at half crack lengths of 8.00, 7.92, 7.84, 7.76, and 7.68 inches. Because the crack turning definition requires two crack tips and the unstable crack growth algorithm is not capable of handling multiple crack tips, only the stable crack growth algorithm is used to analyze the crack turning models. Obtaining meaningful results from only using the stable crack growth algorithm requires the model to have an initial half crack length of six inches. Fortunately, the crack growth curves resulting from an initial half crack length of 2.0 inches and 6.0 inches are similar

for half crack lengths greater than 7.60 inches. The resulting crack growth curves bound the location of crack bifurcation between half crack lengths of 7.76 and 7.84 inches, thereby corroborating the experimental results. Application of three stress based crack turning criteria also corroborates the STAGS results.

After the development of analytical models which correctly predicts the location of crack bifurcation, a parametric study of the effects of tear strap thickness and width on crack bifurcation is performed. New tear strap thicknesses include 0.190, 0.08, 0.04, and 0.02 inches, all based on available aluminum 2024-T3 stock sizes. Changing the tear strap thickness proves to have a significant effect on the crack growth curves near the tear strap. As the thickness decreases, the location of crack bifurcation shifts closer to the edge of the tear strap, the maximum pressure achieved once the crack entered the tear strap decreases, and the minimum pressure on the axial portion of the path decreases. The analysis predicts crack bifurcation in the three largest thicknesses. It is inferred that a 0.02 inch by 2.00 inch tear strap will not cause flapping, instead the tear strap is predicted to fail. The chosen widths are based on integer multiples of the mesh size in the STAGS model, and only widths of 2.0 inches and 0.96 inches are analyzed. These results show that wider tear straps increase the maximum pressure once the crack enters the tear strap, increase the minimum pressure on the axial portion of the path, and shift the location of the crack bifurcation point away from the edge of the tear strap.

6.2 Conclusions

The following are conclusions that have been drawn as a result of this study.

- An analytical model was developed which correctly predicted the fast crack pressure, amount of stable crack growth, and far field circumferential strains of the test article.
- The unstable crack growth algorithm in STAGS was used to generate both the stable and unstable portions of the crack growth curve.
- Self similar crack path results of the complete crack growth curve (stable and unstable portions) indicated that self similar crack growth through a tear strap 0.156 inches thick by 2.0 inches wide is unlikely.

- The point of crack path bifurcation in the experiment was correctly bounded by the analysis which approximated the bifurcating crack path as two oppositely directed circumferentially paths, perpendicular to the initial axial path, emanating from various bifurcation points on the axial path.
- Application of stress based crack turning criteria corroborated the experimental and STAGS crack turning model results.
- For the crack tip close to the tear strap, there are severe in-plane stress gradients through the thickness in the shell wall between the tip and the strap. These stress gradients may cause the crack to slant.
- Decreasing the thickness of the tear strap shifts the location of the crack bifurcation point towards the tear strap, decreases the maximum pressure achieved once the crack enters the strap, and decreases the minimum pressure on the axial portion of the path.
- A tear strap thickness of 0.02 inches and width of 2.0 inches was predicted not to cause flapping, instead the crack was predicted to completely defeat the tear strap.
- Decreasing the width of the tear strap reduces the maximum pressure once the crack entered the tear strap and shifts the location of crack bifurcation closer to the edge of the tear strap.
- From a limited parametric study, it is found that varying the thickness of a tear strap has a larger effect on the behavior of a crack than varying the width of a tear strap.
- In the experiment dynamic crack growth initiates at the relative maximum pressure on the stable part of the crack growth curve. However, the capability of the STAGS code to determine static equilibrium states for different crack paths, including both stable and unstable portions of the path, is demonstrated to be useful in interpreting the efficacy of the tear strap in toughening the structure under dynamic crack growth.

6.3 Future Work

The following are some suggestions for future work on this problem.

- Perform experiments to verify the results presented in this study.

- Replace the assumption of the perfect bond between the cylindrical shell and the tear strap by incorporating an adhesive layer in the model.
- Perform a dynamic crack growth analysis.
- Expand parametric study to include various sizes of cylindrical shells, tear strap materials, tear strap spacing, and different shell/tear strap interfaces.

References

1 Curtis, Howard D., *Fundamentals of Aircraft Structural Analysis*, Irwin, Chicago, IL, 1997, pp. 20-22.

2 Swift, T., "Damage Tolerance in Pressurized Fuselages," *New Materials and Fatigue Resistant Aircraft Design: Proceedings of the 14th Symposium of the International Committee on Aeronautical Fatigue*, (Ottawa, Canada, June 8-12, 1987), Engineering Materials Advisory Services, Cradley Heath, Warley, West Midlands, U.K., 1987, pp 1-77.

3 National Transportation Safety Board, "Aircraft Accident Report Aloha Airlines, Flight 243 Boeing 737-200, N73711, Near Maui, Hawaii, April 28, 1988," Report No. NTSB/AAR-89/03, June 1989.

4 Kanninen, M.F., O'Donoghue, P.E., Green, S.T., Leung, C.P., Roy, S., and Burnside, O.H., "Application of Advanced Fracture Mechanics to Fuselage," Springer Series in Computational Mechanics, 1991, pp. 213-224.

5 Schijve, J., "Fatigue of Aircraft Materials and Structures," *International Journal of Fatigue*, Vol.16, No. 1, 1994, pp. 21-32.

6 Riks, E., Brogan, F.A., and Rankin, C.C., "Bulging of Cracks in Pressurized Fuselages: A Procedure for Computation," in *Analytical and Computational Models of Shells*, edited by A.K. Noor, T. Belytschko, and J.C. Simo, The American Society of Mechanical Engineers, New York, NY, Vol. 3, 1989.

7 Niu, Michael Chun-Yung, "Airframe Structural Design," Conmilit Press Ltd., Hong Kong, 1988, pp. 380-384.

8 Swift, T., "Development of the Fail-safe Design Features of the DC-10," ASTM STP 486, American Society for Testing and Materials, Philadelphia, PA, 1971, pp. 164-214.

9 Folias, E. S., "Fracture in Pressure Vessels," *Thin Shell Structures*, edited by Y. C. Fung and E. E. Sechler, Prentice Hall, Englewood Cliffs, NJ, 1974, pp. 483-518.

10 Duncan, M. E. and Sanders, J. L. Jr., "The Effect of a Circumferential Stiffener on the Stress in a Pressurized Cylindrical Shell with a Longitudinal Crack," *International Journal of Fracture Mechanics*, Vol. 5, 1969, pp. 133-155.

11 Kobayashi, A. S., Emery, A. F., Love, W. J., and Chao, W. -H., “Subsize Experiments and Numerical Modeling of Axial Rupture of Gas Transmission Lines,” *Journal of Pressure Vessel Technology*, Vol. 110, 1988, pp. 155-160.

12 Kosai, M., and Kobayashi, S., “Axial Crack Propagation and Arrest in Pressurized Fuselage,” in *Structural Integrity of Aging Airplanes*, edited by S.N. Atluri, S.G Sampath, and P. Tong, Springer-Verlag, Berlin, Germany, 1991, pp. 225-239.

13 Kosai, M., Shimamoto, A., Yu, C.-T., Walker, S.I., Kobayashi, S. and Tan, P., “Axial Crack Propagation and Arrest in Pressurized Fuselage,” *FAA/NASA International Symposium on Advanced Structural Integrity Methods for Airframe Durability and Damage Tolerance*, NASA Conference Publication 3274, Part 1, 1994, pp. 375-392.

14 Erdogan, F. and Sih, G.C., “On the Crack Extension in Plates Under Plane Loading and Transverse Shear,” *Journal of Basic Engineering*, Vol. 85, 1963, pp. 519-527.

15 Streit, R. and Finnie, I., “An Experimental Investigation of Crack-path Directional Stability,” *Experimental Mechanics*, Vol. 20, 1980, pp. 17-23.

16 Sih, G.C., “Methods of Analysis of Solutions of Crack Problems 1, Edited by G.C. Sih, Noordhoff International Publishing, 1973, pp. 21-45.

17 Wu, C.H., “Fracture Under Combined Loads by Maximum Energy Release Rate Criterion,” *Journal of Applied Mechanics*, Vol. 45, 1978, pp. 553-558.

18 Zaal, K.J.J.M., “A Survey of Crack Path Stability Criteria and Their Application to Crack Flapping Phenomena in Stiffened Structures,” Technical Report LR-681, Faculty of Aerospace Engineering, Technical University of Delft, the Netherlands, 1992.

19 Rankin, C.G., Brogan, F.A., Loden, W.A., and Cabiness, H.D., “STAGS User Manual”, LMMS P032594, March, 1999.

20 Skrzypek, J.J., and Hetnarski, R.B. “Schematizations of the stress-strain curves,” Plasticity and Creep Theory, Examples, and Problems, CRC Press, Inc., Boca Raton, FL, 1993, pp. 43-48.

21 Dawicke, D.S., Sutton, M.A., Newman, J.C., Jr., and Bigelow, C.A., “Measurement and Analysis of Critical CTOA for an Aluminum Allow Sheet,” NASA TM109024, September, 1993.

22 Newman, J. C., Jr., Dawicke, D. S., Sutton, M. A. and Bigelow, C. A., “A Fracture Criterion for Widespread Cracking in Thin-Sheet Aluminum Alloys,” *Durability and Structural Integrity of Airframes: Proceedings of the 17th Symposium of the International Committee on Aeronautical Fatigue*, (Stockholm, Sweden, June 9-11, 1993), Engineering Materials Advisory, Warley, West Midlands, U.K., Vol. 1, 1993, pp. 443-467.

23 Starnes, J. H., Jr., and Rose, C. A., “Buckling and Stable Tearing Responses of Unstiffened Aluminum Shells With Long Cracks,” *The 39th AIAA/ASME/ASCE/ AHS/ASC Structures, Structural Dynamics and Materials Conference and Exhibit*, (Long Beach, California, April, 20-23,1998), American Institute of Aeronautics and Astronautics, Reston, VA, 1998, Part 3, pp. 2389-2402 (AIAA Paper No. 98-1991).

24 Storaasli, Olaf O., “Performance of NASA Equation Solvers on Computational Mechanics Applications,” [online database], URL: http://techre-ports.larc.nasa.gov/ltrs/papers/NASA-aiaa-96-1505/olaf.fm5.html

25 Roark, Raymond J. and Young, Warren C., “Formulas for Stress and Strain,” 5th ed., McGraw-Hill, New York, NY, 1975, pp. 446-455.

26 Rankin, Charles, “Riks Path Parameter Solution Control During Crack Node Release,” Lockheed-Martin Internal Report, Palo Alto, CA, April 1998.

Appendix A

Examples of STAGS Input Files

A.1 Self Similar Crack Growth Input File

```
Pressurized cylinder, perfect bond, experimental tear strap, self
similar crack growth through strap  $A-1
0 0 0                                       $B-1
12 0 0 7 14 0 0 0 1                         $B-2
1 0 2                                       $B-3
26 63  9 63  21 68  26 5  51 7,             $F-1
9 5    5 5   9 7    11 4   4 7,             $F-1
81 7  21 7                                  $F-1
1 3  2 1                                    $G-1
1 4  4 2                                    $G-1
2 4  6 2                                    $G-1
4 3  6 1                                    $G-1
6 3  7 1                                    $G-1
8 1 10 3                                    $G-1
11 3 12 1                                   $G-1
2  9  0 0  3  1  0 0  1 63 1   6 68 1  $G-2
3  5  0 0  7  5  0 0  4  6 1   1  5 2  $G-2
3  0  6 0  7  0  5 0  1  5 1   1  5 1  $G-2
3  5  0 0  8  9  0 0  1  4 1   1  7 2  $G-2
4  0  1 0  5  0  7 0  1 26 1   1 51 2  $G-2
5 11  0 0 11  1  0 0  1  4 1   1  7 2  $G-2
5  0  4 0 11  0  7 0 11 51 1   1 81 2  $G-2
5 51  0 0  9  1  0 0  4  7 1   1  4 1  $G-2
6  0  1 0  9  0  4 0  1  6 1   1 11 2  $G-2
6  0  1 0 10  0  7 0  6  9 1   1  4 1  $G-2
7  0  1 0  8  0  7 0  1  5 1   1  9 2  $G-2
9 11  0 0 10  1  0 0  1  4 1   4  7 1  $G-2
9  0  1 0 12  0  7 0  1 11 1   1 21 2  $G-2
10 1  0 0 12 21  0 0  1  4 1   1  7 2  $G-2
1  4  3  -1  5.00 0 0 2.8                 $G-5
2  5  1 1 11 1                           $G-6
4 11  1 1  5 1                           $G-6
```

```
0 11  6 1 81 1                          $G-6
0 12  1 1 10 1                          $G-6
0  5  1 1 10 1                          $G-7
0 11  1 1 80 1                          $G-7
0 12  1 1  9 1                          $G-7
1 6 0 1 0                               $I-1
10.3594824E6 .30  0.0 .101 12.8E-6 0.0 0.0  $I-2
0.00483  50.0363E3,                     $I-3
0.01500  56.5627E3,                     $I-3
0.04000  62.3640E3,                     $I-3
0.10000  68.1653E3,                     $I-3
0.16000  71.0660E3,                     $I-3
1.00000  72.5163E3                      $I-3
1 1 1 7                                 $K-1
1 .04 0.0  2                            $K-2
2 1 1 7                                 $K-1
1 .196 0.0  2                           $K-2
5 0                                     $M-1 shell unit 1
0.0   8.0 10.0  180.0 9.0               $M-2
1  0 0.0  0.0  0  1                     $M-5
410 0 4 0                               $N-1
30.0  50.0  45.0  45.0                  $N-5
15  20  15  12                          $N-6
4 4 6 6                                 $P-1
1                                       $Q-1
1 1                                     $Q-2
46.52  4  3  0 0 0                      $Q-3
0                                       $R-1
5 0                                     $M-1 shell unit 2
8.0 10.0 10.0  180.0  9.0               $M-2
2 0 0.0 .078 0 1                        $M-5
410 3 4 0                               $N-1
1.60 .32 .08                            $N-2
5 2 1                                   $N-3
30.0  50.0  45.0  45.0                  $N-5
15 20 15 12                             $N-6
6 4 6 6                                 $P-1
1                                       $Q-1
1 1                                     $Q-2
46.52 4 3 0 0  0                        $Q-3
0                                       $R-1
5 0                                     $M-1 shell unit 3
10.0 19.5  0.0  180.0  9.0               $M-2
1 0 0.0 0.0  0 1                        $M-5
410 5 4 1                               $N-1
2.24  1.2  1.5  1.8  2.76               $N-2
7 3 3 3 4                               $N-3
40.0  50.0  45.0  45.0                  $N-5
20 20 15 12                             $N-6
1 5  1 6                                $N-8
6 4 0 4                                 $P-1
100 000                                 $P-2
1                                       $Q-1
1 2                                     $Q-2
```

```
46.52 4 3  0 0  0                    $Q-3
209.34 2 1 21 0  0                   $Q-3
0                                    $R-1
5  0                                 $M-1 shell unit 4
0.0 8.00  6.0  10.0  9.0             $M-2
1  0  0.0  0.0  0 1                  $M-5
410 0 0 0  0 0 0  0 0 0 0            $N-1
4 6 6 6                              $P-1
1                                    $Q-1
1 1                                  $Q-2
46.52  4  3  0 0 0                   $Q-3
0                                    $R-1
5  0                                 $M-1 shell unit 5
0.0  8.0  0.0  6.0  9.0              $M-2
1 0  0.0 0.0  0 1                    $M-5
410 0 0 1  0 0 0  0 1 0 0            $N-1
11 51  1 4                           $N-8
4 6 6 4                              $P-1
1                                    $Q-1
1 1                                  $Q-2
46.52  4 3  0 0  0                   $Q-3
0                                    $R-1
5  0                                 $M-1 shell unit 6
8.0  10.0  6.0  10.0  9.0            $M-2
2 0  0.0 .078 0 1                    $M-5
410 3 0 0  0 0 0  0 0 0 0            $N-1
1.6 .32 .08                          $N-2
5 2 1                                $N-3
6 6 6 6                              $P-1
1                                    $Q-1
1 1                                  $Q-2
46.52  4 3  0 0  0                   $Q-3
0                                    $R-1
5  0                                 $M-1 shell unit 7
10.0 11.28  6.0  10.0  9.0           $M-2
1  0  0.0  0.0  0 1                  $M-5
410 0 0 0  0 0 0  0 0 1 0            $N-1
6 6 6 6                              $P-1
1                                    $Q-1
1 1                                  $Q-2
46.52  4  3  0 0 0                   $Q-3
0                                    $R-1
5  0                                 $M-1 shell unit 8
10.0  11.28  0.0   6.0  9.0          $M-2
1 0  0.0 0.0  0 1                    $M-5
410 0 0 0  0 0 0  0 1 1 0            $N-1
6 6 6 4                              $P-1
1                                    $Q-1
1 1                                  $Q-2
46.52  4 3  0 0  0                   $Q-3
0                                    $R-1
5 0                                  $M-1 shell unit 9
8.0 9.6  3.0  6.0  9.0               $M-2
2 0  0.0 .078 0 1                    $M-5
```

```
410 0 0 0  0 0 0  0 1 0 0              $N-1
6 6 6 6                                $P-1
1                                      $Q-1
1 1                                    $Q-2
46.52  4 3  0 0 0                      $Q-3
0                                      $R-1
5 0                                    $M-1 shell unit 10
9.6 10.0  0.0  6.0  9.0                $M-2
2 0  0.0 .078 0 1                      $M-5
410 2 0 0  0 0 0  0 0 0 0              $N-1
0.32 .08                               $N-2
2 1                                    $N-3
6 6 6 4                                $P-1
1                                      $Q-1
1 1                                    $Q-2
46.52  4 3  0 0 0                      $Q-3
0                                      $R-1
5 0                                    $M-1 shell unit 11
1.60  8.00  0.0  3.0  9.0              $M-2
1 0  0.0 0.0  0 1                      $M-5
410 0 0 0  0 0 0  1 1 0 0              $N-1
6 6 6 4                                $P-1
1                                      $Q-1
1 1                                    $Q-2
46.52  4  3  0 0  0                    $Q-3
0                                      $R-1
5 0                                    $M-1 shell unit 12
8.0 9.6  0.0  3.0  9.0                 $M-2
2 0  0.0 .078 0 1                      $M-5
410 0 0 0  0 0 0  0 1 1 0              $N-1
6 6 6 4                                $P-1
1                                      $Q-1
1 1                                    $Q-2
46.52  4 3  0 0  0                     $Q-3
0                                      $R-1
```

A.2 Turning Crack Input File

```
Crack running and turning to the circumference at x=7.68” perfect bond,
experimental tear strap $A-1
0 0 0                                  $B-1
20 1 0 14 25 -8 0 0 2                  $B-2
1 0 2                                  $B-3
26 62  9 62  21 68  26 7  43 7,        $F-1
9 7    5 7   9 7     5 7   4 7,        $F-1
9 7    7 7   7 7     5 7   5 7,        $F-1
71 7   7 7   5 7     5 7   9 7        $F-1
1 3  2 1                               $G-1
1 4  4 2                               $G-1
2 4  6 2                               $G-1
6 3  7 1                               $G-1
8 1 10 3                               $G-1
9 3 10 1                               $G-1
```

```
11 3 12 1                                          $G-1
C13 3 14 1                                          $G-1
13 4 17 2                                          $G-1
14 4 18 2                                          $G-1
14 3 15 1                                          $G-1
15 4 19 2                                          $G-1
16 3 17 1                                          $G-1
C17 3 18 1                                          $G-1
18 3 19 1                                          $G-1
19 3 20 1                                          $G-1
2  9  0 0  3  1  0 0  1 62 1   7 68 1  $G-2
3  5  0 0  7  5  0 0  4  7 1   1  7 2  $G-2
3  0  7 0  7  0  7 0  1  5 1   1  5 1  $G-2
3  5  0 0  8  9  0 0  1  4 1   1  7 2  $G-2
4  0  1 0  5  0  7 0  1 22 1   1 43 2  $G-2
4 22  0 0 11  1  0 0  1  4 1   4  7 1  $G-2
4  0  4 0 11  0  7 0 22 26 1   1  9 2  $G-2
4 26  0 0  6  1  0 0  4  7 1   4  7 1  $G-2
5 43  0 0 11  1  0 0  4  7 1   1  4 1  $G-2
5 11  0 0 16  1  0 0  1  4 1   1  7 2  $G-2-
5  0  4 0 16  0  7 0 11 43 1   1 65 2  $G-2-
6  0  1 0  9  0  7 0  4  6 1   1  5 2  $G-2
6  0  1 0 10  0  7 0  6  9 1   1  4 1  $G-2
6  4  0 0 12  7  0 0  1  4 1   4  7 1  $G-2
6  0  4 0 12  0  7 0  1  4 1   1  7 2  $G-2
7  0  1 0  8  0  7 0  1  5 1   1  9 2  $G-2
9  1  0 0 20  9  0 0  1  4 1   1  7 2  $G-2-
9  1  0 0 12  7  0 0  4  7 1   1  4 1  $G-2
11 0  1 0 16  0  7 0  1  4 1  65 71 2  $G-2-
11 4  0 0 13  1  0 0  1  4 1   1  7 2  $G-2
11 0  4 0 13  0  7 0  4  7 1   1  7 2  $G-2
11 0  4 0 14  0  7 0  7  9 1   1  5 2  $G-2
12 3  0 0 15  5  0 0  1  4 1   1  7 2  $G-2
12 0  4 0 15  0  7 0  1  3 1   1  5 2  $G-2
12 0  1 0 20  0  7 0  3  7 1   1  9 2  $G-2-
2 11  0 1 0 0                                      $G-3
5   1  1  1  10.0E6                               $G-4
21  1  0  1  -10.0E6                              $G-4
2 11  0 1 0 0                                      $G-3
5   1  1  3  10.0E6                               $G-4
21  1  0  3  -10.0E6                              $G-4
2 70  0 1 0 0                                      $G-3
16  2  1  1  10.0E6                               $G-4
21 12  0  1  -10.0E6                              $G-4
2 70  0 1 0 0                                      $G-3
16  2  1  3  10.0E6                               $G-4
21 12  0  3  -10.0E6                              $G-4
2  6  0 1 0 0                                      $G-3
17  2  1  1  10.0E6                               $G-4
21 82  0  1  -10.0E6                              $G-4
2  6  0 1 0 0                                      $G-3
17  2  1  3  10.0E6                               $G-4
21 82  0  3  -10.0E6                              $G-4
2  3  0 1 0 0                                      $G-3
```

```
18  2  1  1  10.0E6                    $G-4
21 88  0  1  -10.0E6                   $G-4
2  3  0 1 0 0                          $G-3
18  2  1  3  10.0E6                    $G-4
21 88  0  3  -10.0E6                   $G-4
1  5  0   1  2.50                      $G-5
1  5  1 1  11 1  21   1 11 1           $G-6
1 16  2 1  55 1  21  12 65 1           $G-6
0 16 56 1  71 1  21  66 81 1           $G-6
0 17  2 1   6 1  21  82 86 1           $G-6
C0 18  2 1   4 1  21  88 90 1          $G-6
0 17  7 1   7 1  18 1 1  1 1           $G-6
2  3  0   1  5.00 0 0 0 0  10.0E6      $G-5
1 17  7 1  7 1  18 1 1 1 1             $G-6
0 17  7 2  7 7  18 1 2 1 7             $G-6
0 13  7 2  7 7  14 1 2 1 7             $G-6
90                                     $H-1
1 6 0 1 0                              $I-1
10.3594824E6 .30  0.0 .101 12.8E-6 0.0 0.0  $I-2
0.00483  50.0363E3,                    $I-3
0.01500  56.5627E3,                    $I-3
0.04000  62.3640E3,                    $I-3
0.10000  68.1653E3,                    $I-3
0.16000  71.0660E3,                    $I-3
1.00000  72.5163E3                     $I-3
1 1 1 7                                $K-1
1 .04 0.0  2                           $K-2
2 1 1 7                                $K-1
1 .196 0.0  2                          $K-2
5 0                                    $M-1 shell unit 1
0.0   8.0 12.0  180.0 9.0              $M-2
1  0 0.0  0.0  0  1                    $M-5
410 0 4 0                              $N-1
28.0  50.0  45.0  45.0                 $N-5
14  20  15  12                         $N-6
4 4 6 6                                $P-1
1                                      $Q-1
1 1                                    $Q-2
46.52  4  3  0 0 0                     $Q-3
0                                      $R-1
5 0                                    $M-1 shell unit 2
8.0 10.0 12.0  180.0  9.0              $M-2
2 0 0.0 .078 0 1                       $M-5
410 3 4 0                              $N-1
1.60 .32 .08                           $N-2
5 2 1                                  $N-3
28.0  50.0  45.0  45.0                 $N-5
14 20 15 12                            $N-6
6 4 6 6                                $P-1
1                                      $Q-1
1 1                                    $Q-2
46.52 4 3 0 0  0                       $Q-3
0                                      $R-1
5 0                                    $M-1 shell unit 3
```

```
10.0 19.5  0.0  180.0  9.0            $M-2
1 0 0.0 0.0  0 1                     $M-5
410 5 4 1                            $N-1
2.24  1.2  1.5  1.8  2.76            $N-2
7 3 3 3 4                            $N-3
40.0  50.0  45.0  45.0               $N-5
20 20 15 12                          $N-6
1 5  1 7                             $N-8
6 4 0 4                              $P-1
100 000                              $P-2
1                                    $Q-1
1 2                                  $Q-2
46.52 4 3  0 0  0                    $Q-3
209.34 2 1 21 0  0                   $Q-3
0                                    $R-1
5  0                                 $M-1 shell unit 4
0.0 8.00  6.0  12.0  9.0             $M-2
1  0  0.0  0.0  0 1                  $M-5
410 0 0 1  0 0 0  0 0 0 0            $N-1
22 26  1 4                           $N-8
4 6 6 6                              $P-1
1                                    $Q-1
1 1                                  $Q-2
46.52  4  3  0 0 0                   $Q-3
0                                    $R-1
5  0                                 $M-1 shell unit 5
0.0  6.72  0.0  6.0  9.0             $M-2
1 0  0.0 0.0  0 1                    $M-5
410 0 0 1  0 0 0  0 1 0 0            $N-1
11 45  1 4                           $N-8
4 6 6 3                              $P-1
1                                    $Q-1
1 1                                  $Q-2
46.52  4 3  0 0  0                   $Q-3
0                                    $R-1
5  0                                 $M-1 shell unit 6
8.0  10.0  6.0  12.0  9.0            $M-2
2 0  0.0 .078 0 1                    $M-5
410 3 0 1  0 0 0  0 0 0 0            $N-1
1.6 .32 .08                          $N-2
5 2 1                                $N-3
1 4  1 4                             $N-8
6 6 6 6                              $P-1
1                                    $Q-1
1 1                                  $Q-2
46.52  4 3  0 0  0                   $Q-3
0                                    $R-1
5  0                                 $M-1 shell unit 7
10.0 11.28  6.0  12.0  9.0           $M-2
1  0  0.0  0.0  0 1                  $M-5
410 0 0 0  0 0 0  0 0 1 0            $N-1
6 6 6 6                              $P-1
1                                    $Q-1
1 1                                  $Q-2
```

```
46.52  4  3  0 0 0                    $Q-3
0                                     $R-1
5  0                                  $M-1 shell unit 8
10.0  11.28  0.0   6.0  9.0           $M-2
1 0  0.0 0.0  0 1                     $M-5
410 0 0 0  0 0 0  0 1 1 0             $N-1
6 6 6 4                               $P-1
1                                     $Q-1
1 1                                   $Q-2
46.52  4 3  0 0  0                    $Q-3
0                                     $R-1
5 0                                   $M-1 shell unit 9
8.96 9.6  0.0  6.0  9.0               $M-2
2 0  0.0 .078 0 1                     $M-5
410 0 0 0  0 0 0  0 1 0 0             $N-1
6 6 6 4                               $P-1
1                                     $Q-1
1 1                                   $Q-2
46.52  4 3  0 0 0                     $Q-3
0                                     $R-1
5 0                                   $M-1 shell unit 10
9.6 10.0  0.0  6.0  9.0               $M-2
2 0  0.0 .078 0 1                     $M-5
410 2 0 0  0 0 0  0 0 0 0             $N-1
0.32 .08                              $N-2
2 1                                   $N-3
6 6 6 4                               $P-1
1                                     $Q-1
1 1                                   $Q-2
46.52  4 3  0 0 0                     $Q-3
0                                     $R-1
5 0                                   $M-1 shell unit 11
6.72 8.00  3.0 9.0  9.0               $M-2
1 0  0.0 0.0  0 1                     $M-5
410 0 0 1  0 0 0  0 1 0 0             $N-1
4 9  1 4                              $N-8
6 6 6 6                               $P-1
1                                     $Q-1
1 1                                   $Q-2
46.52  4 3  0 0  0                    $Q-3
0                                     $R-1
5 0                                   $M-1 shell unit 12
8.0 8.96  3.0  9.0  9.0               $M-2
2 0  0.0 .078 0 1                     $M-5
410 0 0 1  0 0 0  0 1 0 0             $N-1
1 3  1 4                              $N-8
6 6 6 6                               $P-1
1                                     $Q-1
1 1                                   $Q-2
46.52  4 3  0 0  0                    $Q-3
0                                     $R-1
5 0                                   $M-1 shell unit 13
7.20 7.68  3.0 6.0  9.0               $M-2
1 0  0.0 0.0  0 1                     $M-5
```

```
410 0 0 0  0 0 0  1 1 0 0          $N-1
6 6 6 6                            $P-1
1                                  $Q-1
1 1                                $Q-2
46.52  4 3  0 0  0                 $Q-3
0                                  $R-1
5 0                                $M-1 shell unit 14
7.68 8.00  3.0 6.0  9.0            $M-2
1 0  0.0 0.0  0 1                  $M-5
410 0 0 0  0 0 0  0 1 0 0          $N-1
6 6 6 6                            $P-1
1                                  $Q-1
1 1                                $Q-2
46.52  4 3  0 0  0                 $Q-3
0                                  $R-1
5 0                                $M-1 shell unit 15
8.0 8.32  3.0  6.0  9.0            $M-2
2 0  0.0 .078 0 1                  $M-5
410 0 0 0  0 0 0  0 1 1 0          $N-1
6 6 6 6                            $P-1
1                                  $Q-1
1 1                                $Q-2
46.52  4 3  0 0  0                 $Q-3
0                                  $R-1
5 0                                $M-1 shell unit 16
1.60  7.20  0.0  3.0  9.0          $M-2
1 0  0.0 0.0  0 1                  $M-5
410 0 0 0  0 0 0  1 1 0 0          $N-1
6 6 6 3                            $P-1
1                                  $Q-1
1 1                                $Q-2
46.52  4  3  0 0  0                $Q-3
0                                  $R-1
5 0                                $M-1 shell unit 17
7.20 7.68  0.0 3.0  9.0            $M-2
1 0  0.0 0.0  0 1                  $M-5
410 0 0 0  0 0 0  0 0 0 0          $N-1
6 6 6 3                            $P-1
1                                  $Q-1
1 1                                $Q-2
46.52  4 3  0 0  0                 $Q-3
0                                  $R-1
5 0                                $M-1 shell unit 18
7.68 8.00  0.0 3.0  9.0            $M-2
1 0  0.0 0.0  0 1                  $M-5
410 0 0 0  0 0 0  0 0 0 0          $N-1
6 6 6 3                            $P-1
1                                  $Q-1
1 1                                $Q-2
46.52  4 3  0 0  0                 $Q-3
0                                  $R-1
5 0                                $M-1 shell unit 19
8.0 8.32  0.0  3.0  9.0            $M-2
2 0  0.0 .078 0 1                  $M-5
```

```
410 0 0 0  0 0 0  0 0 0 0              $N-1
6 6 6 4                                $P-1
1                                      $Q-1
1 1                                    $Q-2
46.52  4 3  0 0  0                     $Q-3
0                                      $R-1
5 0                                    $M-1 shell unit 20
8.32 8.96  0.0  3.0  9.0               $M-2
2 0  0.0 .078 0 1                      $M-5
410 0 0 0  0 0 0  0 1 1 0              $N-1
6 6 6 4                                $P-1
1                                      $Q-1
1 1                                    $Q-2
46.52  4 3  0 0  0                     $Q-3
0                                      $R-1
1  0 0 0  0.0 0.0 9.0  101 010  0  10  $S-1 nodes unit 5
1  0 0 0  .16 0.0 0.0                  $S-1a
11 0 0 0  1.6 0.0 9.0  101 010  0  80  $S-1 nodes units 16-18
1  0 0 0  .08 0.0 0.0                  $S-1a
1                                      $U-1
1 1                                    $U-2
46.52  4  3  0  0 0                    $U-3
0                                      $V-1
```

A.3 Solution Input File

```
Solution input file with the new unstable crack growth prodecure, X_ck
$A-1
3  1  0 0 0 0 0 1                      $B-1  NONLINEAR ANALYSIS
1 0                                    $B-2  VSS
0.1      .01  1.5                     $C-1
0   0     50 -20 -1                    $D-1
0                                      $ET-1

Solution input file with only the stable crack growth prodecure
$A-1
3  1  0 0 0 0 0 1                      $B-1  NONLINEAR ANALYSIS
1 0                                    $B-2  VSS
0.1      .01  1.5                     $C-1
0   0     50 -20 -1                    $D-1
0                                      $ET-1
```

Appendix B

Parametric Study: Results from the Stress Based Crack Turning Criterion

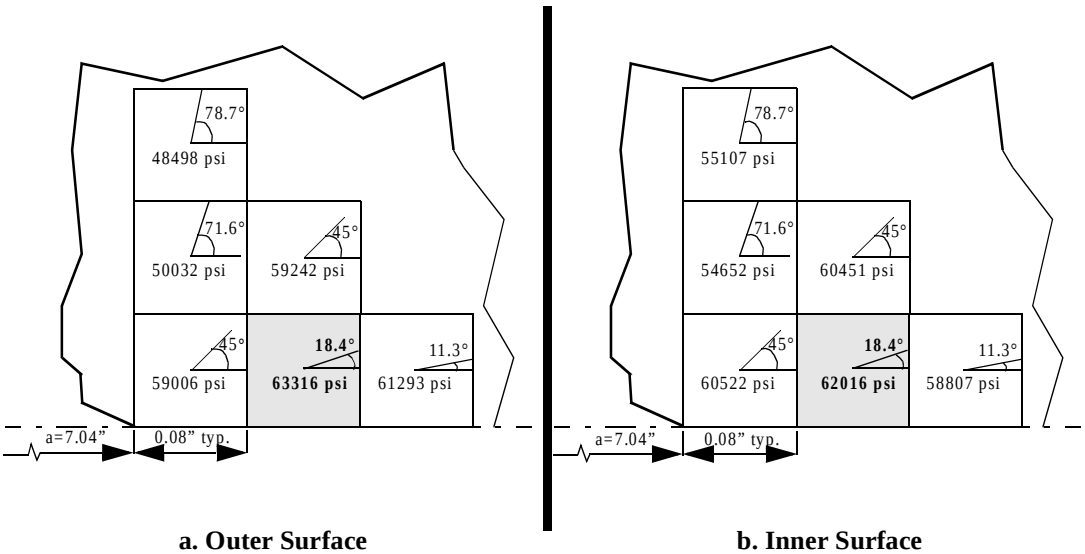

a. Outer Surface **b. Inner Surface**

Crack growth direction is axial.

Fig. B.1 Maximum polar normal stress criterion for a 0.04 in. by 2.0 in. tear strap, a=7.04 in.

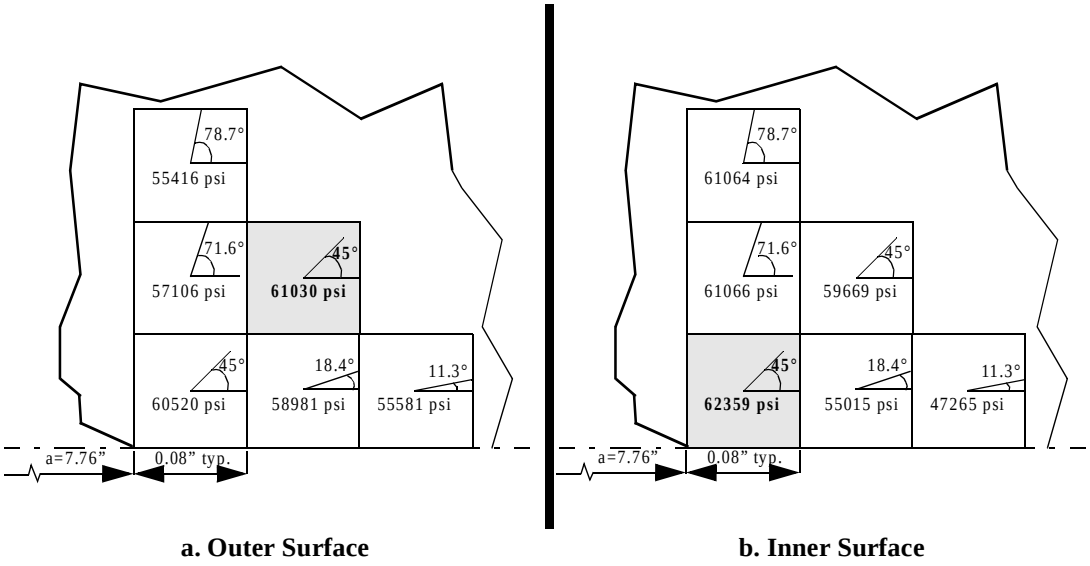

a. Outer Surface **b. Inner Surface**

Direction of crack growth is inconclusive.

Fig. B.2 Maximum polar normal stress criterion for a 0.04 in. by 2.0 in. tear strap, a=7.76 in.

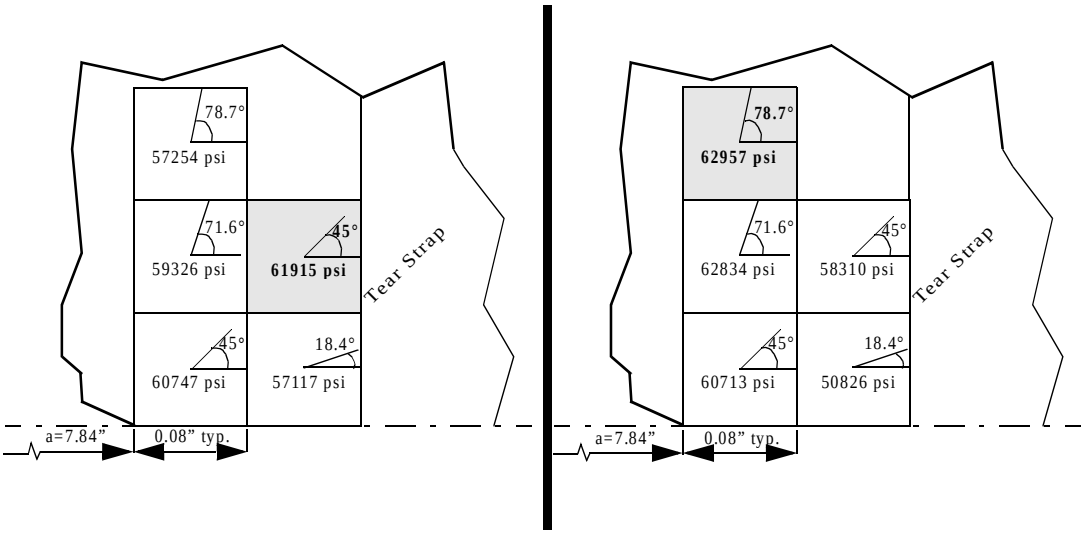

a. Outer Surface **b. Inner Surface**

Direction of crack growth is inconclusive.

Fig. B.3 Maximum polar normal stress criterion for a 0.04 in. by 2.0 in. tear strap, a=7.84 in.

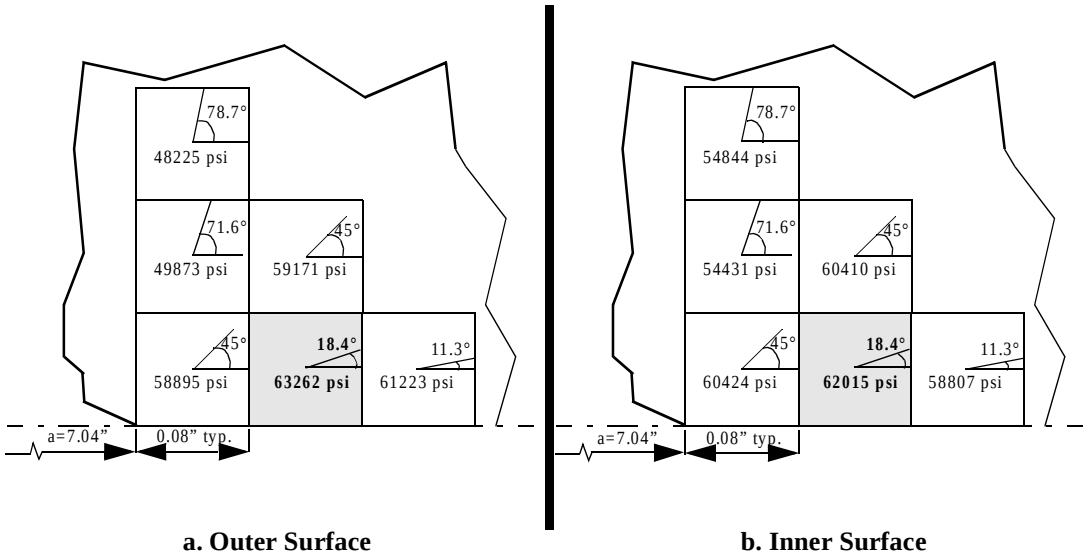

a. Outer Surface **b. Inner Surface**

Crack growth direction is axial.

Fig. B.4 Maximum polar normal stress criterion for a 0.02 in. by 2.0 in. tear strap, a=7.04 in.

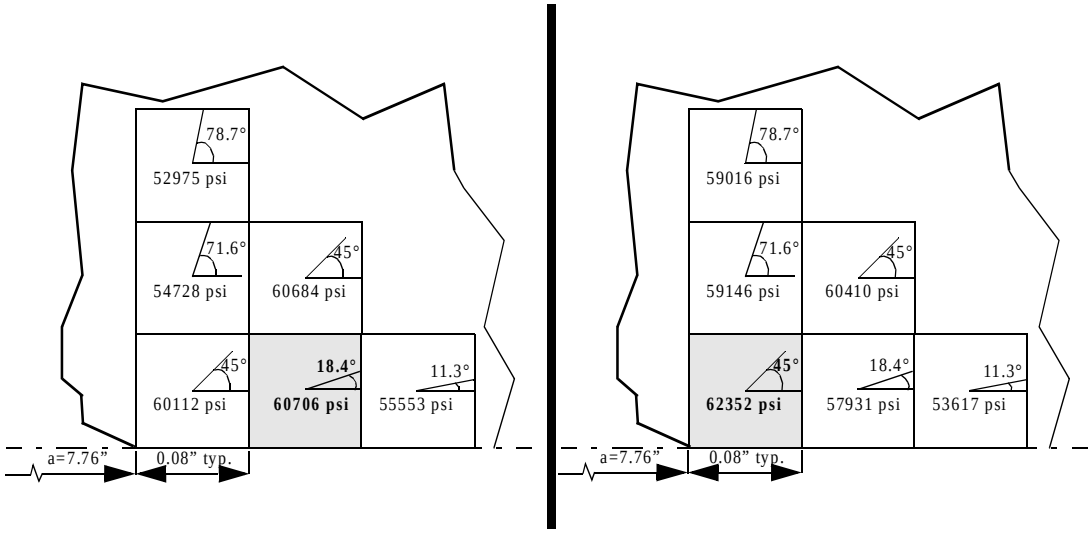

a. Outer Surface **b. Inner Surface**

Direction of crack growth is inconclusive.

Fig. B.5 Maximum polar normal stress criterion for a 0.02 in. by 2.0 in. tear strap, a=7.76 in.

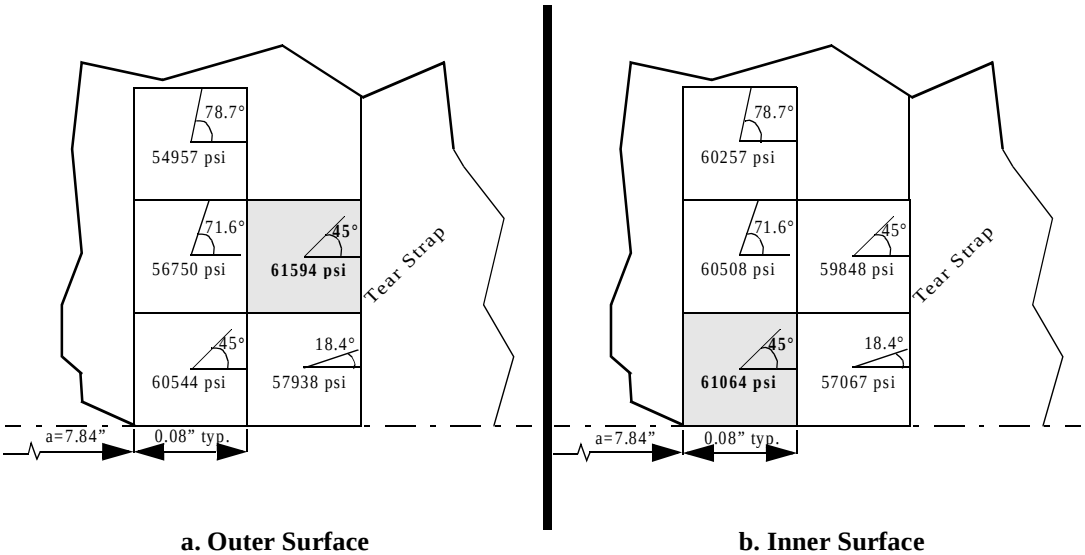

a. Outer Surface **b. Inner Surface**

Direction of crack growth is inconclusive.

Fig. B.6 Maximum polar normal stress criterion for a 0.02 in. by 2.0 in. tear strap, a=7.84 in.

Vita

Amy L. Cowan was born and raised in Western Pennsylvania. After graduation from high school, she attended the Pennsylvania State University majoring in Aerospace Engineering. While at Penn State, she earned a Cooperative Education position at the NASA Langley Research Center. After graduation and working a year and a half as a design engineer at MicroCraft, Inc., she enrolled in the Department of Aerospace and Ocean Engineering at Virginia Tech with the goal of earning a Masters of Science degree. Upon completion of the MS requirements, the author will be employed by the Naval Surface Warfare Center, Carderock Division.